Delays Induce Novel Stochastic Effects in Negative Feedback Gene Circuits

Eder Zavala and Tatiana T. Marquez-Lago*

Integrative Systems Biology Unit, Okinawa Institute of Science and Technology, Okinawa, Japan
* Correspondence: tatiana.marquez@oist.jp

SUPPORTING MATERIAL

Supporting Tables and Models

1. **Biological Ranges for Parameter Values and Sets of Fixed Nominal Values for Oscillatory and Multimodal Regimes** (TABLES S1 – S3)
2. **Continuous Deterministic Model**
3. **Discrete Stochastic Model**

Supporting Text

1. **About the Hopf Bifurcation**
2. **Period Estimation of Stochastic Oscillations**

Supporting Figures

FIGURE S1 – The deterministic bifurcation analysis evidences a Hopf bifurcation.

FIGURE S2 – Comparison between deterministic and stochastic sample trajectories.

FIGURE S3 – Delay Stochastic Simulation Algorithm (DSSA) based on the Reaction Rejection Method.

FIGURES S4-S10 – Samples of stochastic realizations and probability density functions for different feedback strengths and transcriptional delay values.

FIGURE S11 – Sample stochastic oscillations and amplitude distributions.

FIGURE S12 – Period estimation from frequency spectra obtained by FFT.

FIGURES S13-S19 – Autocorrelation functions and their half-lives for different feedback strengths and transcriptional delay values.

FIGURES S20-S21 – Sample stochastic oscillations for a simulation volume of 5 fL and 37 fL, respectively.

FIGURES S22-S23 – Sample stochastic trajectories showing multimodality for a simulation volume of 5 fL and 37 fL, respectively.

Supporting Tables and Models

1. Biological Ranges for Parameter Values and Sets of Fixed Nominal Values for Oscillatory and Multimodal Regimes

Parameter	Description	Value	Units
k_1	Transcription rate	10/60	s^{-1}
k_2	Translation rate	10/60	s^{-1}
k_d^+	Dimer association rate	$5*10^7$	$M^{-1}s^{-1}$
k_d^-	Dimer dissociation rate	1	s^{-1}
k_c^+	Dimer-DNA binding rate	10^8	$M^{-1}s^{-1}$
k_c^-	Dimer-DNA unbinding rate	k_c^+ / α	s^{-1}
γ_1	mRNA degradation rate	10^{-2}	s^{-1}
γ_2	Protein degradation rate	10^{-2}	s^{-1}

TABLE S1 Parameter set used for describing the onset of oscillations. For consistency, parameter values are identical to the ones used in a previous work (see Parameter Set 1 in (1)). The only exception is γ_2, which was increased from 10^{-4} to 10^{-2} s^{-1} to observe self-sustained oscillations in the deterministic model.

Parameter	Description	Value	Tolerance	Units
k_1	Transcription rate	1/60	1/60 – 10/60	s^{-1}
k_2	Translation rate	10/60	1/60 – 10/60	s^{-1}
k_d^+	Dimer association rate	10^7	$10^5 – 5*10^7$	$M^{-1}s^{-1}$
k_d^-	Dimer dissociation rate	10^2	$1 – 10^2$	s^{-1}
k_c^+	Dimer-DNA binding rate	10^{10}	-	$M^{-1}s^{-1}$
k_c^-	Dimer-DNA unbinding rate	k_c^+ / α	-	s^{-1}
α	Feedback strength	10^{15}	$10^{13} – 10^{15}$	M^{-1}
γ_1	mRNA degradation rate	10^{-5}	$10^{-4} – 10^{-5}$	s^{-1}
γ_2	Protein degradation rate	10^{-2}	-	s^{-1}

TABLE S2 Parameter set used for describing multimodality. Tolerances describe the range of values where multimodal behavior is still observed. An important exception is γ_1, which drives the system to bursty expression if increased from its nominal value.

Parameter	Description	Range	Units
k_1	Transcription rate	$10^{-3} – 2*10^{-1}$	s^{-1}
k_2	Translation rate	$10^{-3} – 1$	s^{-1}
k_d^+	Dimer association rate	$5*10^7 – 3*10^8$	$M^{-1}s^{-1}$
k_d^-	Dimer dissociation rate	$1 – 10^3$	s^{-1}
k_c^+	Dimer-DNA binding rate	$10^8 – 2*10^{11}$	$M^{-1}s^{-1}$
k_c^-	Dimer-DNA unbinding rate	k_c^+ / α	s^{-1}
α	Feedback strength	$10^{-20} – 10^{15}$	M^{-1}
γ_1	mRNA degradation rate	$10^{-4} – 10^{-1}$	s^{-1}
γ_2	Protein degradation rate	$2*10^{-5} – 10^{-2}$	s^{-1}
τ_1	Transcription delay	0 – 1500	s
τ_2	Translation delay	10 – 150	s

TABLE S3 Biological ranges of parameter values used in the present study (1, 2).

2. Continuous Deterministic Model

Considerations

- Modeled as a continuous deterministic DDE system with two discrete constant delays.
- No Quasi Steady-State (QSS) assumption was adopted.
- No lumping of transcription-translation processes.
- DNA, mRNA, Protein and Dimer concentrations are considered explicitly.

Reactions and Model

Starting from the set of reactions Eq. 1 in the main text, let molecular concentrations be denoted by

g = [DNA] m = [mRNA] d = [D] $g_{total} = g + g_b$ = constant
g_b = [DNA•D] p = [P]

The corresponding system of ODEs is

$$\begin{aligned}\dot{g} &= k_c^- g_b - k_c^+ g d \\ \dot{m} &= k_1 g - \gamma_1 m \\ \dot{p} &= k_2 m - \gamma_2 p + k_d^- d - k_d^+ p^2 \\ \dot{d} &= k_c^- g_b - k_c^+ g d + k_d^+ p^2 - k_d^- d\end{aligned} \qquad \text{Eq. S1}$$

where k_1 and k_2 are the transcription and translation rates, respectively. Dimer association/dissociation rates are denoted by k_d^+ and k_d^-; a dimer binds and unbinds DNA at rates k_c^+ and k_c^-; whereas mRNA and protein turnover are represented by rates γ_1 and γ_2, respectively. Replacing the conservation equation and introducing time delays we arrive to the system of DDEs

$$\begin{aligned}\dot{g} &= k_c^+\left(\frac{g_{tot} - g}{\alpha} - g d\right) \qquad \alpha = k_c^+ / k_c^- \\ \dot{m} &= k_1 g_{\tau_1} - \gamma_1 m \\ \dot{p} &= k_2 m_{\tau_2} - \gamma_2 p + k_d^- d - k_d^+ p^2 \\ \dot{d} &= k_c^+\left(\frac{g_{tot} - g}{\alpha} - g d\right) + k_d^+ p^2 - k_d^- d\end{aligned} \qquad \text{Eq. S2}$$

where τ_1 and τ_2 are, respectively, the delays of the transcription and translation processes defined as $x_\tau = x(t-\tau)$.

Parameters

To explore how the solutions of the system depend qualitatively on parameter values, that is, a bifurcation analysis, we adopted the set of parameter values in Table S1. All kinetic rate constants except for γ_2 take the same value as in the "Basic Simulation Parameter Set 1" described in Table S2 of (1). The parameter γ_2 corresponds to the protein degradation rate. In our simulations, this parameter required a two-fold increase to observe deterministic self-sustained oscillations. However, the value used here still lies within biologically feasible ranges (see Table S3 and (1)).

3. Discrete Stochastic Model

Considerations

- Modeled through an implementation of the Delay Stochastic Simulation Algorithm (DSSA) that reproduces exact trajectories of the Delay Chemical Master Equation (DCME). Transcription and translation delays were treated as constant.
- No Quasi Steady-State (QSS) assumption was adopted.
- No lumping of transcription-translation processes.
- DNA, mRNA, Protein, Dimer and Repression Complex (DNA-Dimer) concentrations are considered explicitly.

Reactions and Model

Starting from the set of reactions Eq. 1 in the main text, lets split them into the following set of individual reactions

$$\begin{aligned} DNA &\rightarrow DNA + mRNA \\ mRNA &\rightarrow mRNA + P \\ P + P &\rightarrow D \\ D &\rightarrow P + P \\ DNA + D &\rightarrow Complex \\ Complex &\rightarrow DNA + D \\ mRNA &\rightarrow \varnothing \\ P &\rightarrow \varnothing \end{aligned} \qquad \text{Eq. S3}$$

From Eq. S3, we can build an *m x n* matrix corresponding to *m* reactions and *n* molecular species, each entry denoting the discrete change in the amount of molecular species *n* after the *m* reaction occurred. This is the stoichiometric matrix S of the system, which, together with the reaction delays vector T, is given by

$$S = \begin{pmatrix} 0 & 1 & 0 & 0 & 0 \\ 0 & 0 & 1 & 0 & 0 \\ 0 & 0 & -2 & 1 & 0 \\ 0 & 0 & 2 & -1 & 0 \\ -1 & 0 & 0 & -1 & 1 \\ 1 & 0 & 0 & 1 & -1 \\ 0 & -1 & 0 & 0 & 0 \\ 0 & 0 & -1 & 0 & 0 \end{pmatrix}, \qquad T = \begin{pmatrix} \tau_1 \\ \tau_2 \\ 0 \\ 0 \\ 0 \\ 0 \\ 0 \\ 0 \end{pmatrix}. \qquad \text{Eq. S4}$$

Following this, the reaction propensities are described in vector A as

$$A = \begin{pmatrix} k_1 \cdot DNA \\ k_2 \cdot mRNA \\ \left(k_d^+/\sigma\right) \cdot P(P-1)/2 \\ k_d^- \cdot D \\ \left(k_c^+/\sigma\right) \cdot DNA \cdot D \\ \left(k_c^+/\alpha\right) \cdot Complex \\ \gamma_1 \cdot mRNA \\ \gamma_2 \cdot P \end{pmatrix} \qquad \text{Eq. S5}$$

where k_1 and k_2 are the transcription and translation rates, respectively. Dimer association/dissociation rates are denoted by k_d^+ and k_d^-; a dimer binds and unbinds DNA at rates k_c^+ and k_c^-; whereas mRNA and protein turnover are represented by rates γ_1 and γ_2, respectively. The parameter σ is the product of Avogadro's number with the volume of one femtoliter, and was used to convert from molarity units.

The stoichiometric matrix S, together with the propensities A, the vector T and a set of initial conditions, are necessary inputs for carrying out realizations of trajectories of the DCME through the DSSA (Fig. S3). All reactions were treated as non-consuming reactions.

Parameters

The parameters used in the stochastic description are the same as in the deterministic one (Table S1). It was only required to convert from molarity units after considering the size of the system, corresponding to the volume a typical *E. coli* cell (1 fL) (3).

Scaling-up the Size of the System: From Prokaryotes to Eukaryotes

Some of the parameter values considered here lie within ranges that are also valid for eukaryotes. This is particularly true for the transcriptional delay, spanning values as high as 20 min. We wondered if our stochastic model predictions regarding oscillations and multistability would hold for such systems of larger size.

Thus, we decided to test our model and carried out stochastic simulations using a volume of 5 fL and 37 fL (see parameter σ in Eq. S5). These values correspond, respectively, to the maximum volume for an *E. coli* cell (3) and to the mean volume for a typical *S. cerevisiae* cell (4). All other parameter values were taken from Tables S1 and S2 for oscillations and multimodality, respectively. We carried out stochastic simulations using the same methods and protocols already described in the main text. For testing oscillations, however, we only explored transcriptional delay values in the highest portion of the range (τ_1 = 800 s and τ_1 = 1200 s).

Some resulting stochastic trajectories exhibiting oscillations and multimodality are shown in Figs. S20-S21 and Figs. S22-S23, respectively. Thus, though our model predictions may differ in magnitude between prokaryote and eukaryote systems, they're qualitatively equivalent.

Supporting Text

1. About the Hopf Bifurcation

Consider a dynamical system that depends on parameters. In general, we represent such a system as $\dot{x} = f(x,\alpha)$ or $\dot{x} \mapsto f(x,\alpha)$ in the continuous- and discrete-time case, respectively. There, $x \in \mathbb{R}^n$ and $\alpha \in \mathbb{R}^m$ stand for the phase variables and parameters, respectively. The state of the system at time t is thus the collection of values its phase variables take at that time. Depending on how the state changes over time and its response to perturbations, they are referred as stable/unstable equilibrium states (steady-states), periodic orbits, and other more sophisticated classifications. The collection of states that a system exhibits can be represented in a phase portrait of the system. As the parameters vary, the phase portrait also varies. In some cases, the phase portrait remains topologically equivalent, but in others, it can undergo sudden qualitative changes in the system's set of solutions. Following this, the appearance of a topologically nonequivalent phase portrait under variation of parameters is called a bifurcation (5). In other words, the bifurcation is a change in the dynamical regime of the system as its parameters pass through a critical value.

Bifurcation theory deals with describing the qualitative dynamical changes that can be observed in a system as its parameters vary. For example, after varying one or more parameters, the state of the system may change from stable to unstable and/or a periodic solution may arise. The relationship between the network architecture of the system (i.e. the wiring among its variables as judged by the graph representation of the Jacobian matrix), the topology invariance of phase portraits as parameters vary (i.e. the robustness of the system), and the many different types of bifurcations described so far, is an active topic of research.

A Hopf bifurcation, such as the one mentioned in this article, occurs when a steady-state changes its stability at a critical parameter value and low-amplitude oscillations, described by a limit cycle, emerge at the same time. In deterministic systems, this is verified by the presence of a purely imaginary pair of eigenvalues of the Jacobian matrix evaluated at the equilibrium point (5) (Fig. S1, *C*). If only one parameter is varied in the search of novel qualitative solutions for the system, the bifurcation occurs at a critical point, which is called a *bifurcation point*. If two parameters are varied, the bifurcation occurs at a critical line (a one-dimensional manifold), which here is simply called a *bifurcation branch*. In this article, each Hopf bifurcation branch illustrated in Fig. 2 is a set of (τ_1, α) values defining the boundary between a stable steady-state solution and a periodic one. For the special case where $\tau_1 = \tau_2 = 0$, the system of DDEs becomes a set of Ordinary Differential Equations (ODEs). We confirmed that its time-course evolution always converged to a stable steady-state solution by numerically solving the ODE system using the parameter set in Table S1 and performing parameter sweeps of the feedback strength within the range $\alpha \in [10^7, 10^{15}]$ M^{-1} (data not shown). The monostable and oscillatory scenarios were both verified by numerical computations of time-course trajectories (Figs. S1 *F* and S2) as described in the Methods section.

In stochastic systems, however, bifurcation theory is not yet fully developed. Thus, to tell whether a stochastic Hopf bifurcation has occurred one can inspect the stationary Probability Density Functions (PDFs) as its shape changes from unimodal to bimodal. In our system, the basal expression state is located at a low non-zero value (see for instance the unimodal distributions in Fig. S4). When the (τ_1, α) values are increased, this state eventually vanishes while oscillations emerge in its place. This is reflected by the corresponding PDFs widening and flattening around the position of the former basal state. The emergent oscillations have its crests reaching higher values as the bifurcation parameters increase, while its troughs reach zero values all the time (molecule numbers are positively defined). As a consequence, a great portion of the PDFs is hoarded by the first, lower mode. Higher transcriptional delays transform the PDFs from a flattened to a bimodal shape, making it clearer that the transition from basal state to the oscillatory has completed (see Figs. S4 to S10 and notice that only the second mode is represented when PDFs become bimodal). Conversely to the deterministic analysis, the definition of a critical stochastic bifurcation point (or branch) doesn't exist. Other arbitrary criteria, such as the one chosen in this work, must be used to judge whether a new stochastic dynamical regime has emerged. We believe our criterion of observing bimodal PDFs is stringent enough to assert stochastic oscillations emerged through a delay-induced stochastic Hopf bifurcation.

2. Period Estimation of Stochastic Oscillations

To estimate oscillation periods, frequency spectra were calculated for each trajectory by means of a Fast Fourier Transform (FFT) algorithm and its inverse (period curve) averaged for each batch of 100 trajectories. In each case, the period was calculated as the value of the highest local maximum. It is worth noting we made an exception for $\alpha = 10^{12}$ M^{-1}, where identification of local maxima became problematic (Fig. S12). In that case, we first made a rough estimation of the period by measuring the crest-to-crest distance in the corresponding time-course trajectories. We then calculated the period by identifying the highest local maxima in the period spectra that was close to our previous estimation.

Unfortunately, we could not use such a strategy with feedback strength values beyond $\alpha = 10^{12}$ M^{-1}. The latter was due to the very irregular and sparse distribution of peaks in time-course trajectories. These observations suggest that this feedback strength value defines a frontier between stochastic oscillations and bursty dynamics. In Fig. 4, *D*–*F*, the period distributions for mRNA, protein and dimer are shown as functions of τ_1 and α. There, we can see a steep and steady increment in period as the feedback strength and transcription delay increases. Period calculations for $\alpha > 10^{12}$ M^{-1} were omitted for the above mentioned reasons.

Supporting Figures

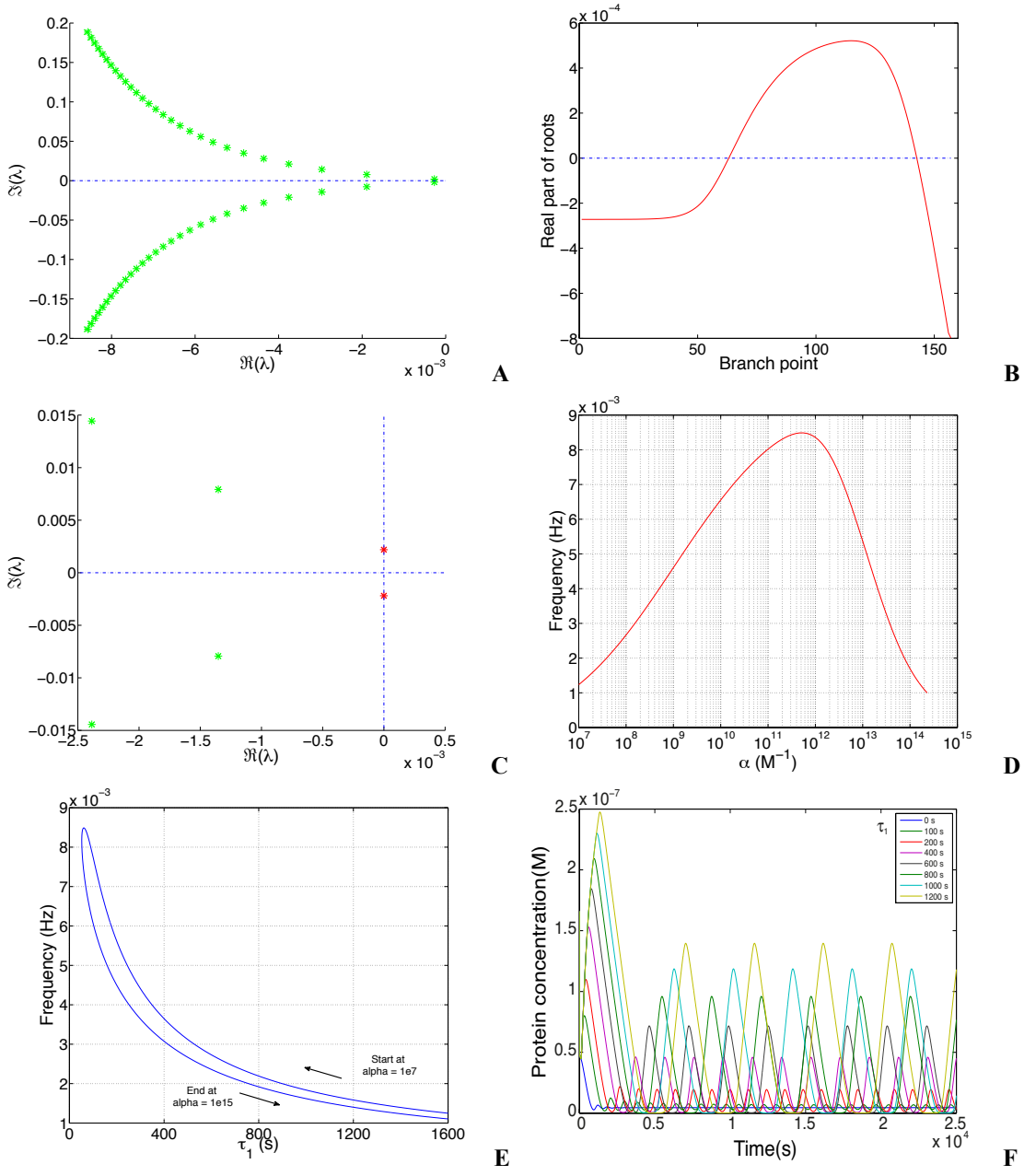

FIGURE S1 The bifurcation analysis evidences a Hopf bifurcation. (A) First eigenvalues of the steady-state used as seed for continuation of the steady-state branch. As all eigenvalues show negative real parts, the steady-state is stable. (B) Continuation of the stability branch of steady-states. The change in sign of roots as a function of branch points reveals critical points where the steady-state change its stability. (C) The roots of the leftmost critical point touch the imaginary axis, evidencing a Hopf bifurcation. This critical point is used for continuation of the Hopf branch $\tau_2 = 100$ s in Fig. 2. The same result is obtained if the rightmost critical point is used for continuation (not shown). (D) Frequency of the nascent periodic solution along the Hopf branch as a function of α and (E) the transcription delay τ_1. (F) Time-course evolution of the deterministic system for different τ_1 values using the parameter set in Table S1 and fixed $\alpha = 10^{11}$ M^{-1}.

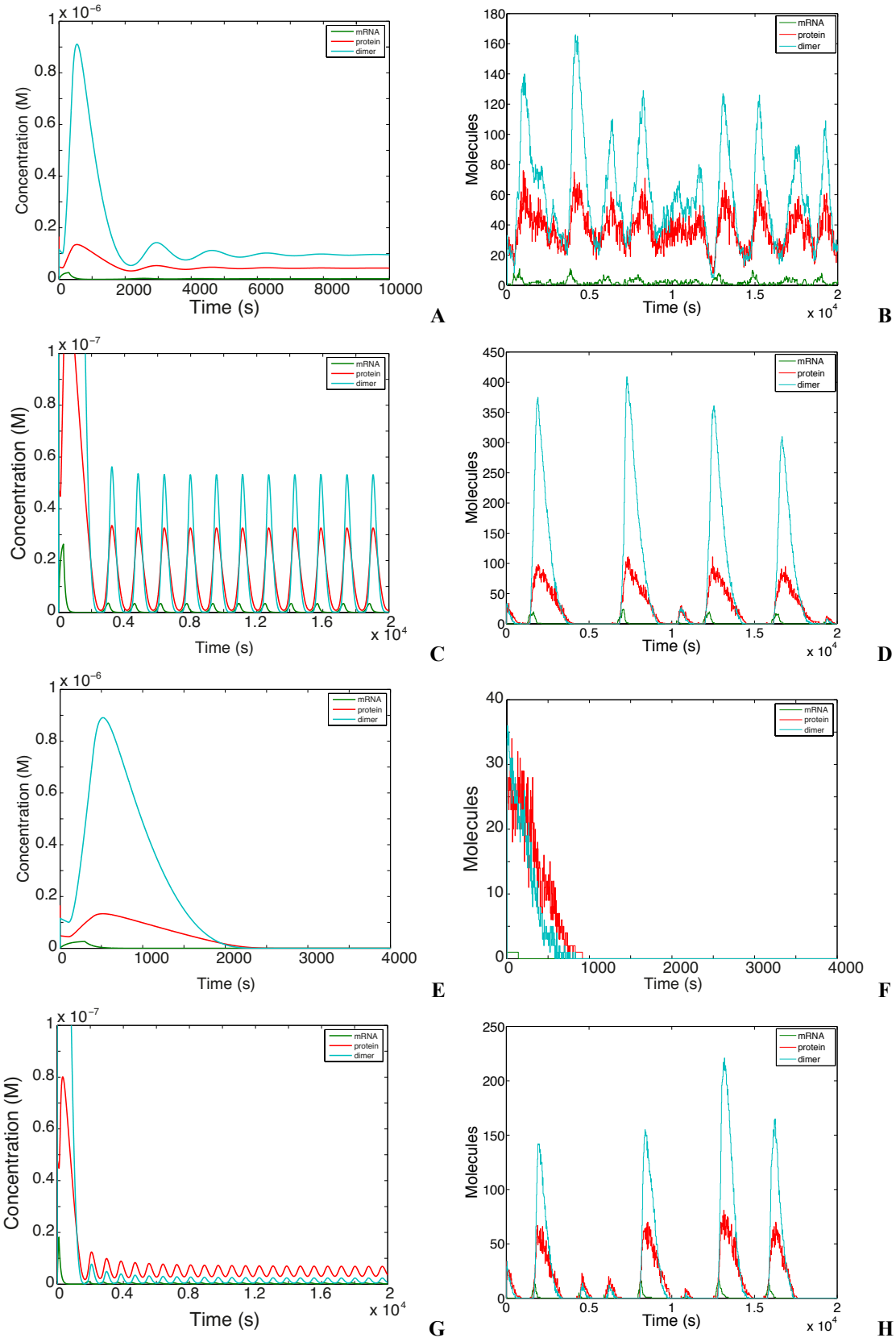

FIGURE S2 Qualitative comparison of sample time-course trajectories: deterministic (*left column*) and stochastic (*right column*). Translation delay was fixed at τ_2 = 100 s while feedback strength and transcriptional delay were set to (A, B) $\alpha = 10^8$ M^{-1}, τ_1 = 300 s; (C, D) $\alpha = 10^{11}$ M^{-1}, τ_1 = 300 s; (E, F) $\alpha = 10^{15}$ M^{-1}, τ_1 = 300 s and (G, H) $\alpha = 10^{11}$ M^{-1}, α_1 = 100 s.

INPUT DATA: Reactions defined by reactant and product vectors. Reactions are tagged as non-delayed or delayed. If delayed, reactions are tagged as consuming or non-consuming. Stoichiometry. Reaction rates. Initial state X(0). Simulation time T. Delays.

RESULT: State dynamics.

PSEUDO-CODE:

```
begin
  while t < T do

    generate U1 and U2 as U(0,1) random variables
    a0(X(t)) = sum{j=1:m,aj(X(t))}
    θ = ln{1/U1}/a0(X(t))
    select j such that
      sum{k=1:j-1,ak(X(t))} < U2*a0(X(t)) ≤ sum{k=1:j,ak(X(t))}

    if delayed reactions are scheduled within (t,t+θ] then
      let k be the delayed reaction scheduled next at time t+τ
      if k is a consuming delayed reaction then
        X(t+τ) = X(t) + υk^p  (update products only)
      else
        X(t+τ) = X(t) + υk
      t = t + τ

    else

      if j is not a delayed reaction then
        X(t+θ) = X(t) + υj
      else
        record time t + θ + τj for delayed reaction j with delay τj
        if j is a consuming delayed reaction then
          X(t+θ) = X(t) + υj^r  (update reactants)
      t = t + θ

end
```

FIGURE S3 Delay Stochastic Simulation Algorithm. The algorithm is based on the reaction rejection method and accounts for consuming and non-consuming reactions. In contrast to the Gillespie SSA, the DSSA makes explicit distinction between reaction waiting times (θ, *in blue*) and reaction delays (τ, *in red*). This algorithm was proved to yield exact trajectories from the DCME in (6). Pseudo-code reproduced from (7).

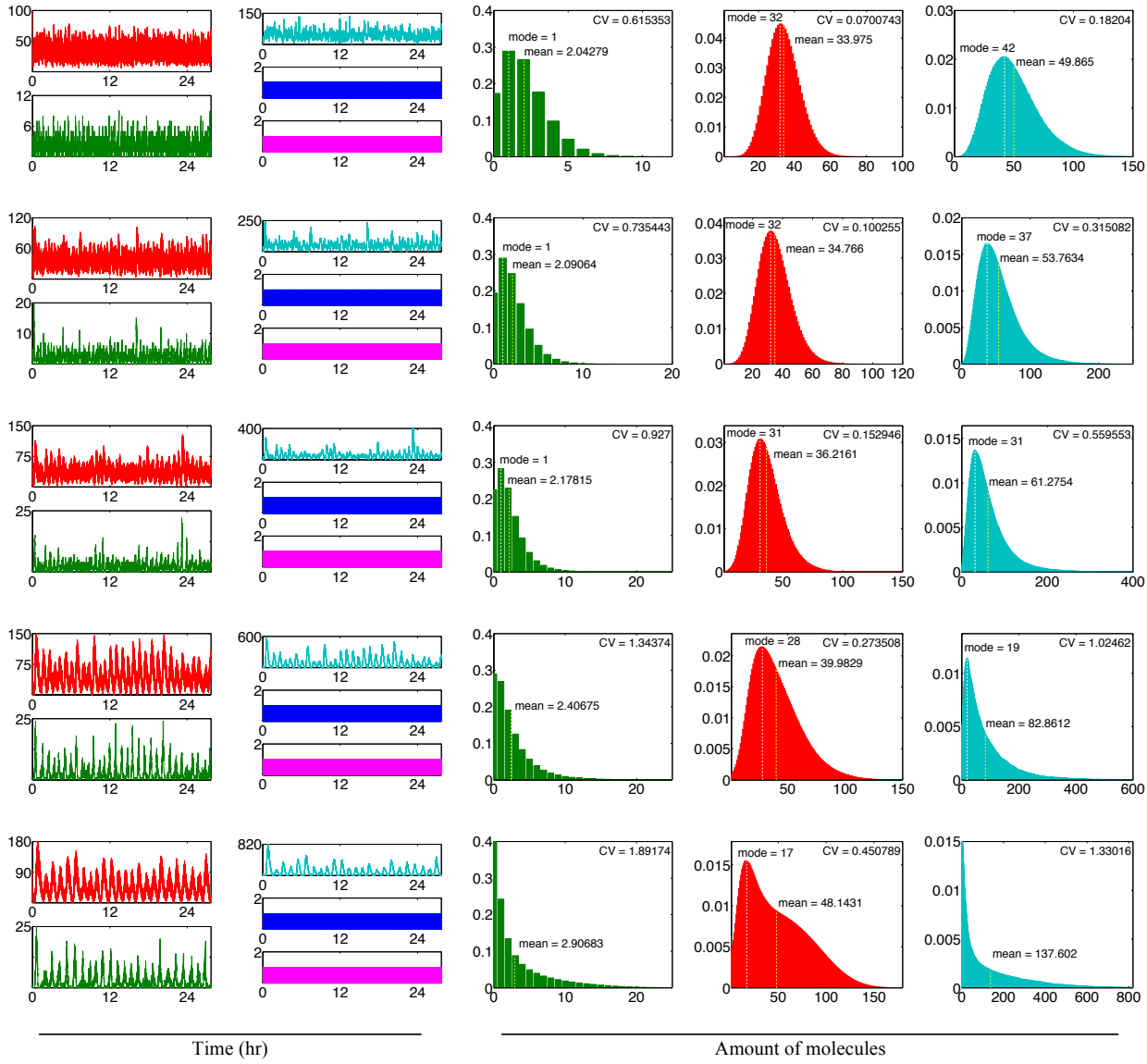

FIGURE S4 Sample stochastic trajectories (*first two columns*) and stationary PDFs over 100 stochastic trajectories (*last three columns*) for feedback strength fixed at $\alpha = 10^8$ M^{-1}. Each row corresponds to a different feedback transcription delay, from top to bottom: $\tau_1 = 100$ s, $\tau_1 = 300$ s, $\tau_1 = 500$ s, $\tau_1 = 800$ s and $\tau_1 = 1200$ s. Protein, mRNA, dimer, DNA and the repressed complex are shown in red, green, teal, blue and pink, respectively.

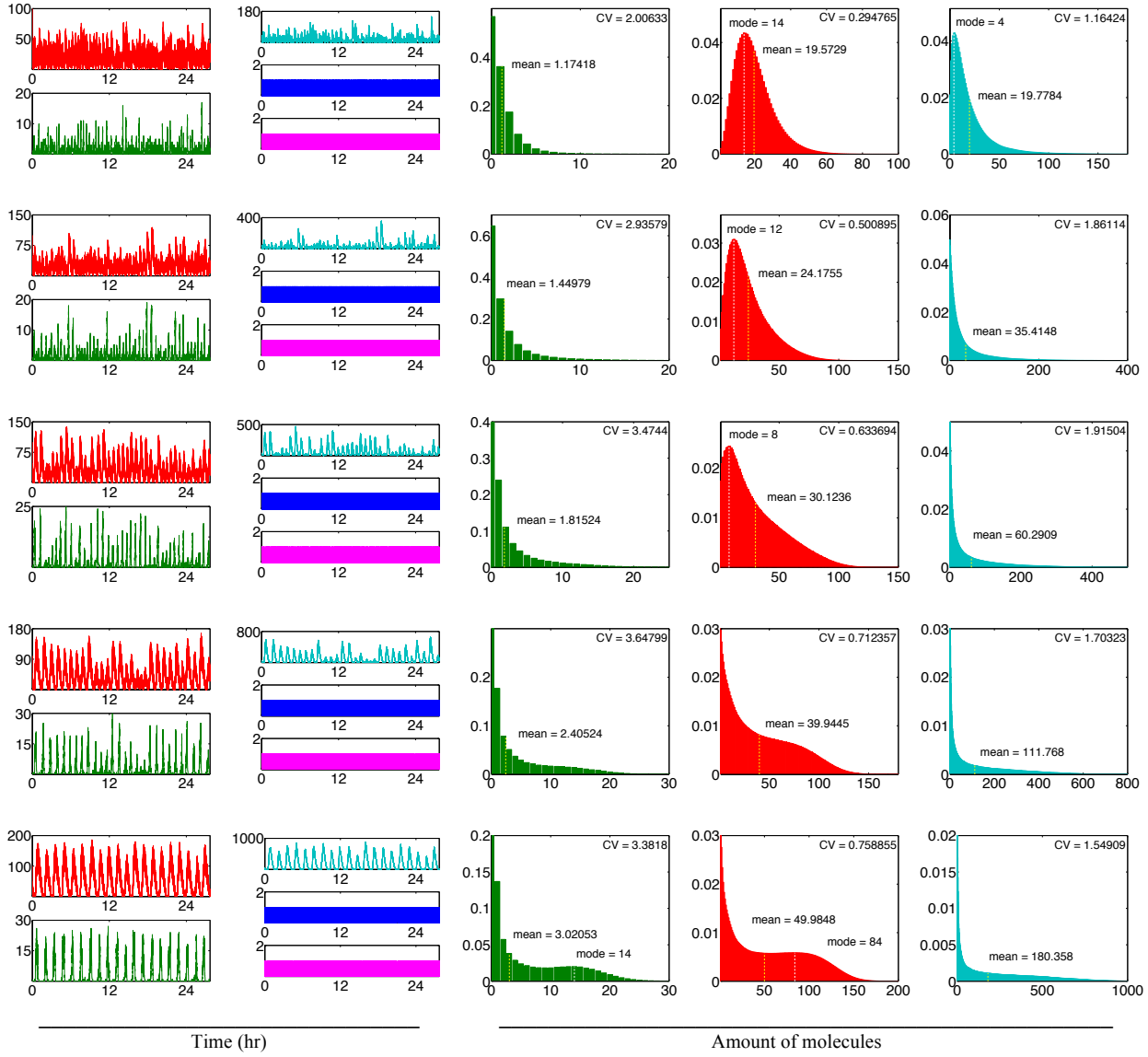

FIGURE S5 Sample stochastic trajectories (*first two columns*) and stationary PDFs over 100 stochastic trajectories (*last three columns*) for feedback strength fixed at $\alpha = 10^9$ M^{-1}. Each row corresponds to a different feedback transcription delay, from top to bottom: $\tau_1 = 100$ s, $\tau_1 = 300$ s, $\tau_1 = 500$ s, $\tau_1 = 800$ s and $\tau_1 = 1200$ s. Protein, mRNA, dimer, DNA and the repressed complex are shown in red, green, teal, blue and pink, respectively.

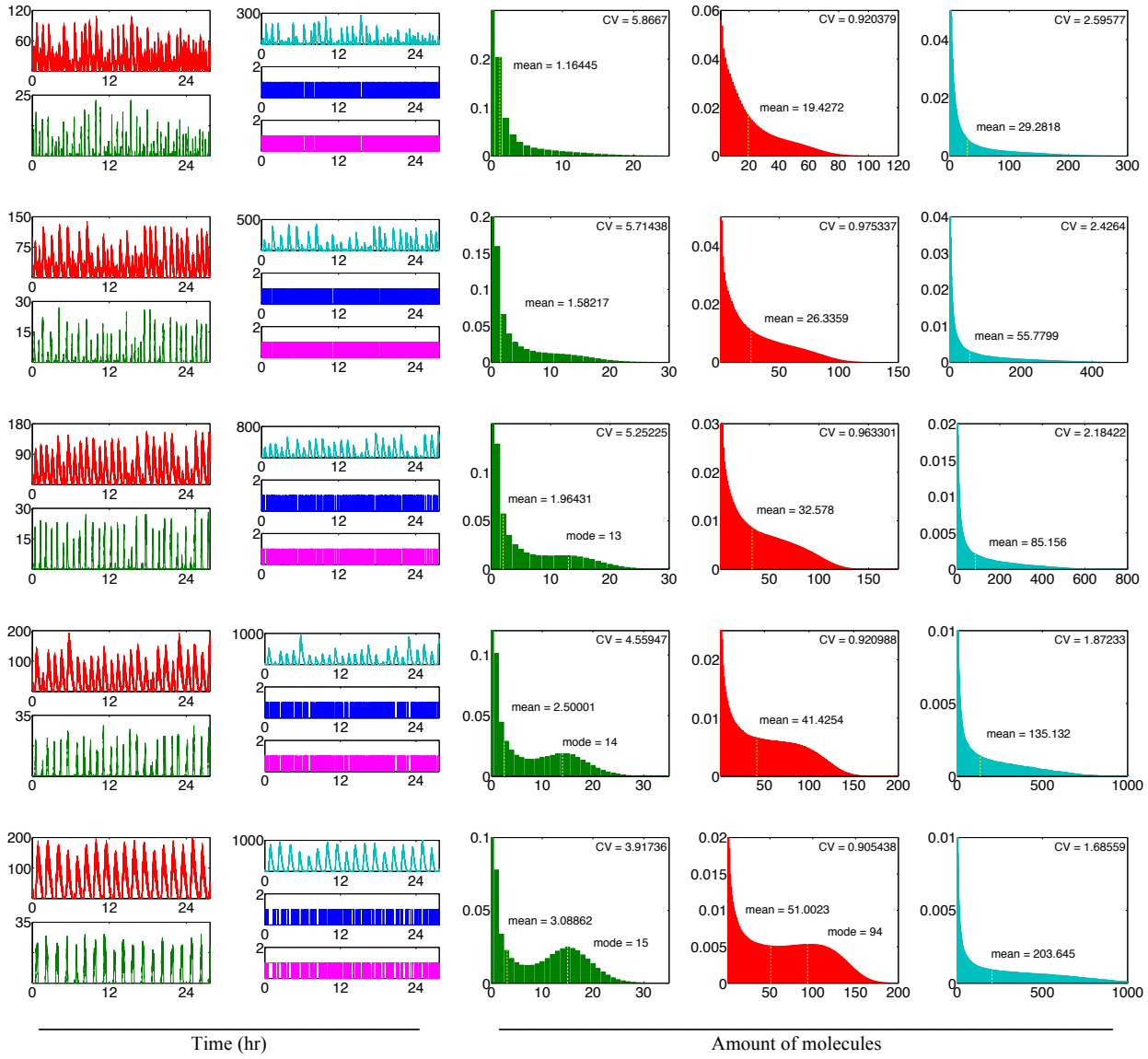

FIGURE S6 Sample stochastic trajectories (*first two columns*) and stationary PDFs over 100 stochastic trajectories (*last three columns*) for feedback strength fixed at $\alpha = 10^{10}$ M^{-1}. Each row corresponds to a different feedback transcription delay, from top to bottom: $\tau_1 = 100$ s, $\tau_1 = 300$ s, $\tau_1 = 500$ s, $\tau_1 = 800$ s and $\tau_1 = 1200$ s. Protein, mRNA, dimer, DNA and the repressed complex are shown in red, green, teal, blue and pink, respectively.

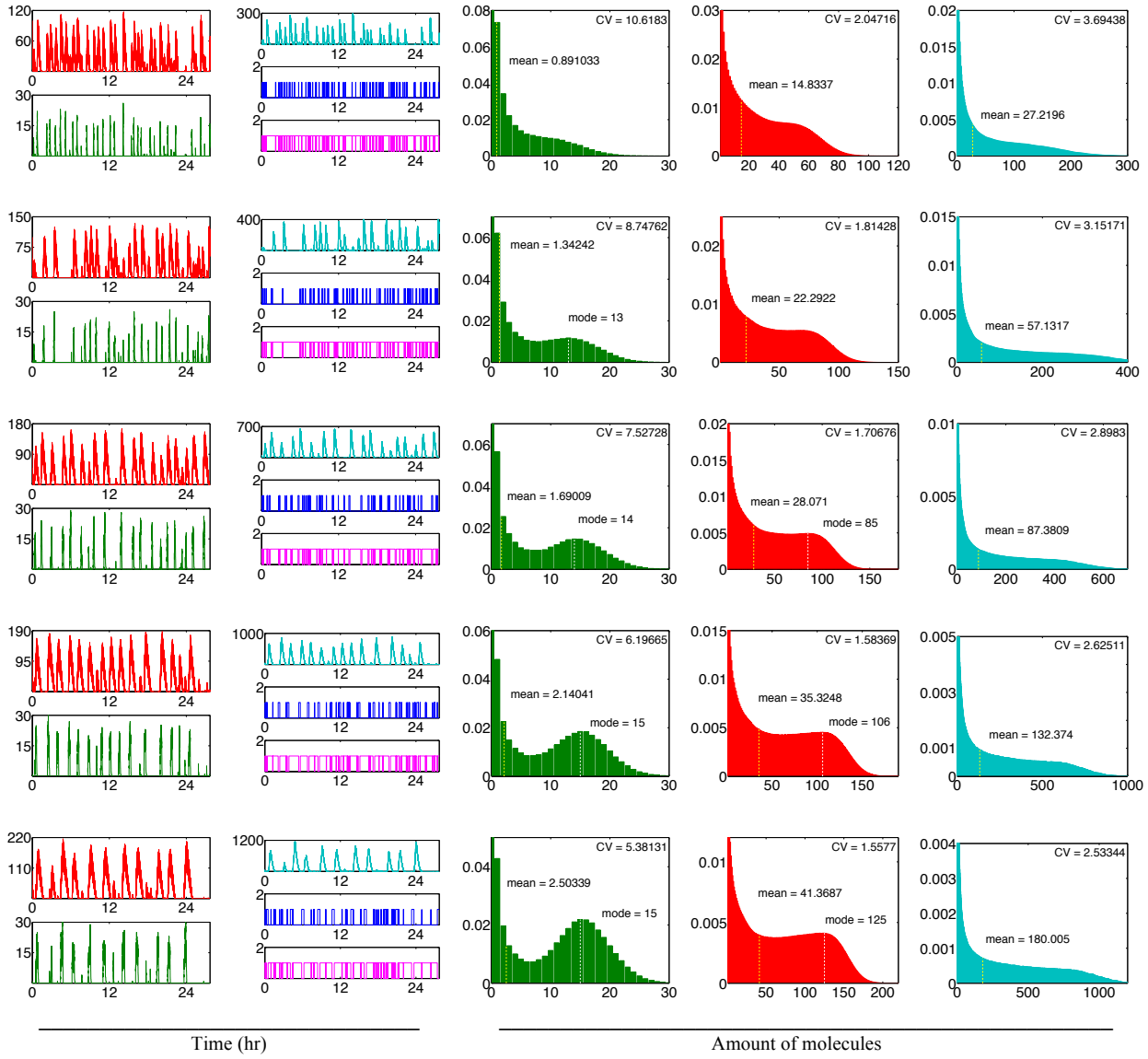

FIGURE S7 Sample stochastic trajectories (*first two columns*) and stationary PDFs over 100 stochastic trajectories (*last three columns*) for feedback strength fixed at $\alpha = 10^{11}$ M^{-1}. Each row corresponds to a different feedback transcription delay, from top to bottom: $\tau_1 = 100$ s, $\tau_1 = 300$ s, $\tau_1 = 500$ s, $\tau_1 = 800$ s and $\tau_1 = 1200$ s. Protein, mRNA, dimer, DNA and the repressed complex are shown in red, green, teal, blue and pink, respectively.

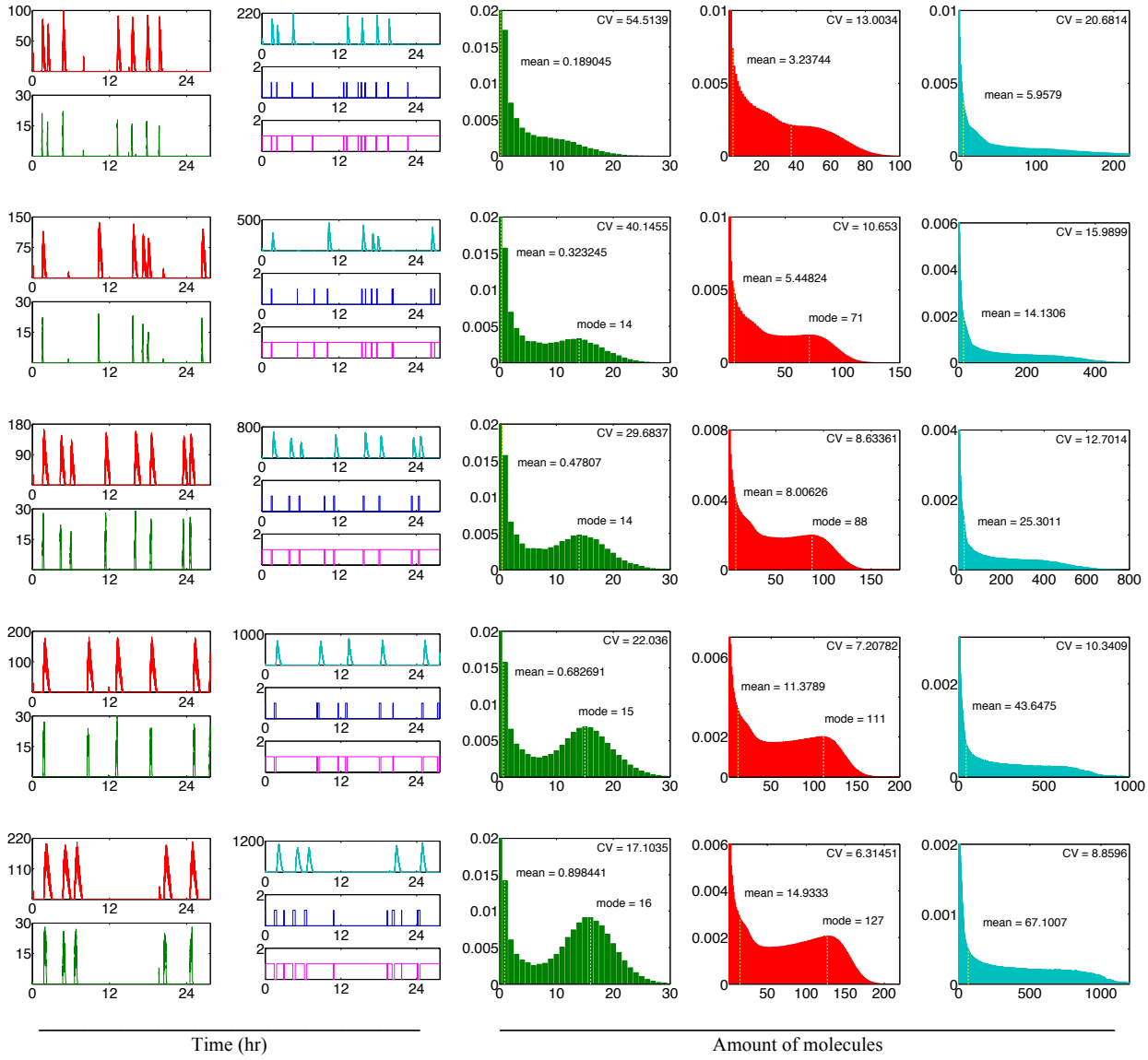

FIGURE S8 Sample stochastic trajectories (*first two columns*) and stationary PDFs over 100 stochastic trajectories (*last three columns*) for feedback strength fixed at $\alpha = 10^{12}$ M^{-1}. Each row corresponds to a different feedback transcription delay, from top to bottom: $\tau_1 = 100$ s, $\tau_1 = 300$ s, $\tau_1 = 500$ s, $\tau_1 = 800$ s and $\tau_1 = 1200$ s. Protein, mRNA, dimer, DNA and the repressed complex are shown in red, green, teal, blue and pink, respectively.

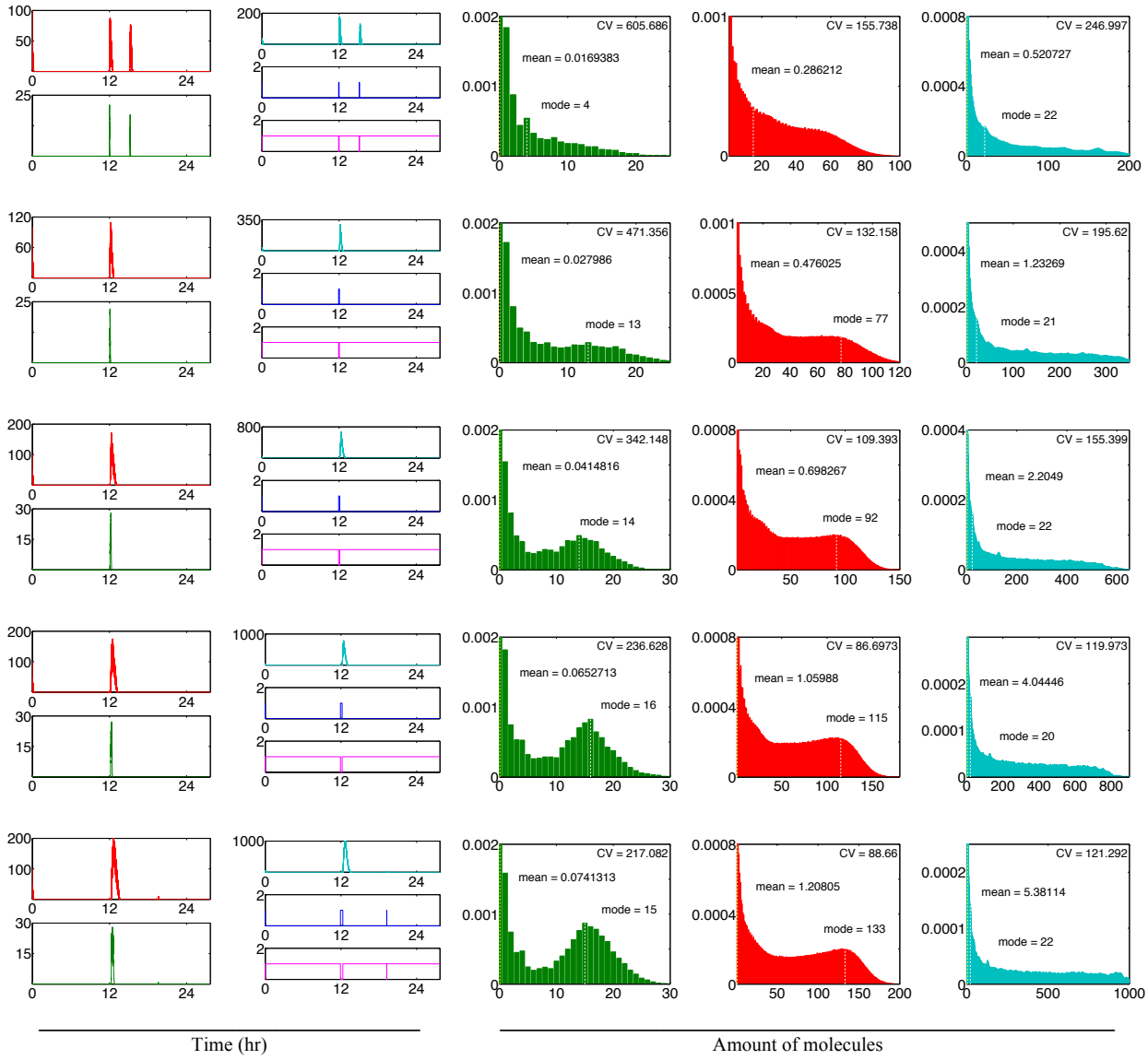

FIGURE S9 Sample stochastic trajectories (*first two columns*) and stationary PDFs over 100 stochastic trajectories (*last three columns*) for feedback strength fixed at $\alpha = 10^{13}$ M^{-1}. Each row corresponds to a different feedback transcription delay, from top to bottom: $\tau_1 = 100$ s, $\tau_1 = 300$ s, $\tau_1 = 500$ s, $\tau_1 = 800$ s and $\tau_1 = 1200$ s. Protein, mRNA, dimer, DNA and the repressed complex are shown in red, green, teal, blue and pink, respectively.

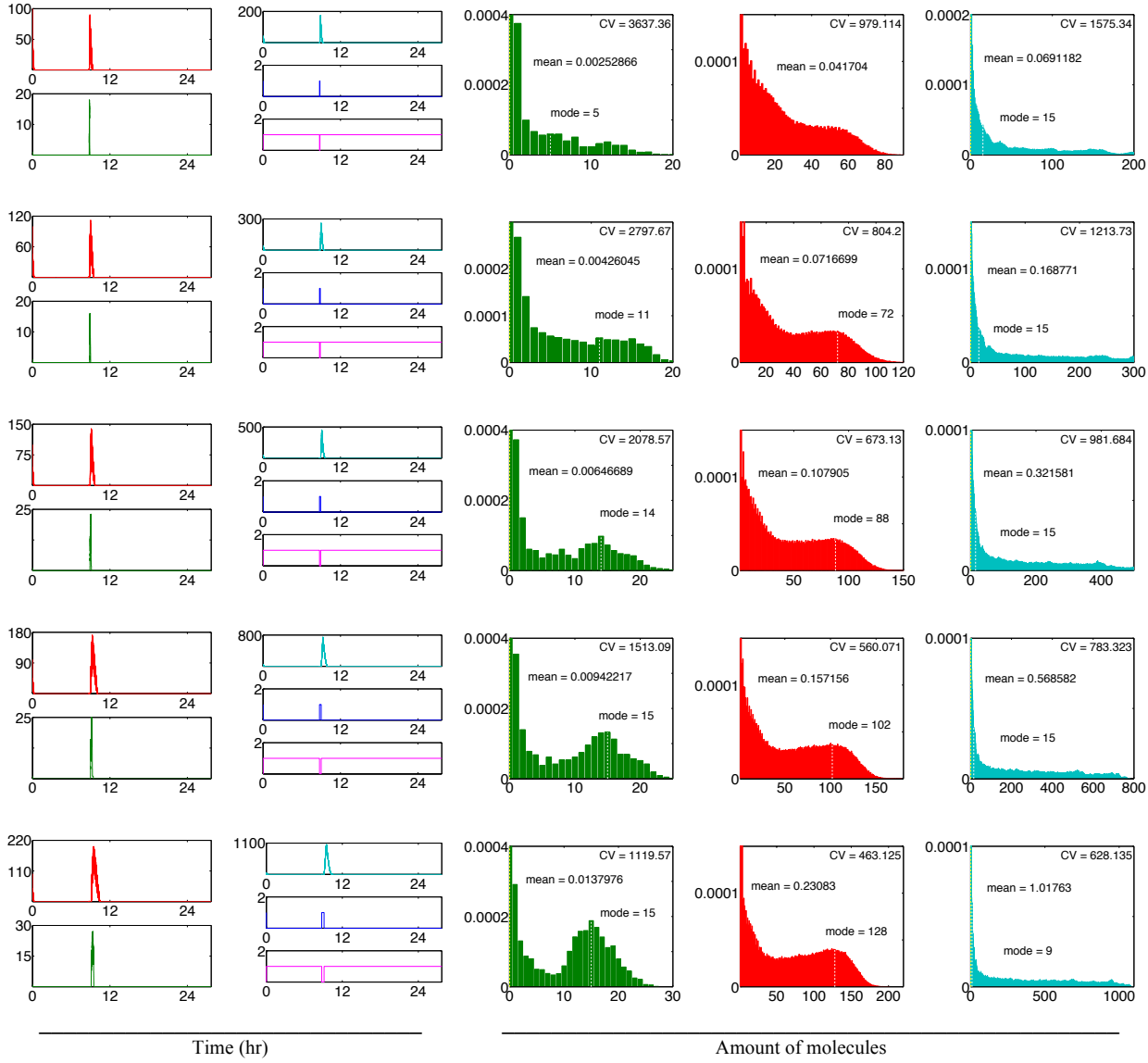

FIGURE S10 Sample stochastic trajectories (*first two columns*) and stationary PDFs over 100 stochastic trajectories (*last three columns*) for feedback strength fixed at $\alpha = 10^{14}$ M^{-1}. Each row corresponds to a different feedback transcription delay, from top to bottom: $\tau_1 = 100$ s, $\tau_1 = 300$ s, $\tau_1 = 500$ s, $\tau_1 = 800$ s and $\tau_1 = 1200$ s. Protein, mRNA, dimer, DNA and the repressed complex are shown in red, green, teal, blue and pink, respectively.

FIGURE S11 Sample stochastic realizations (*time-course trajectories*) and amplitude distributions over 100 stochastic trajectories (*horizontal histograms*). All vertical axes represent molecule numbers. Each row corresponds to different feedback strengths, from top to bottom: $\alpha = 10^{8}$ M^{-1}, $\alpha = 10^{9}$ M^{-1}, $\alpha = 10^{10}$ M^{-1}, $\alpha = 10^{11}$ M^{-1}, $\alpha = 10^{12}$ M^{-1}, $\alpha = 10^{13}$ M^{-1} and $\alpha = 10^{14}$ M^{-1}. Each column corresponds to a different transcription delay, from left to right: $\tau_1 = 100$ s, $\tau_1 = 300$ s, $\tau_1 = 500$ s, $\tau_1 = 800$ s and $\tau_1 = 1200$ s. Protein, mRNA and dimer are shown in red, green and teal, respectively.

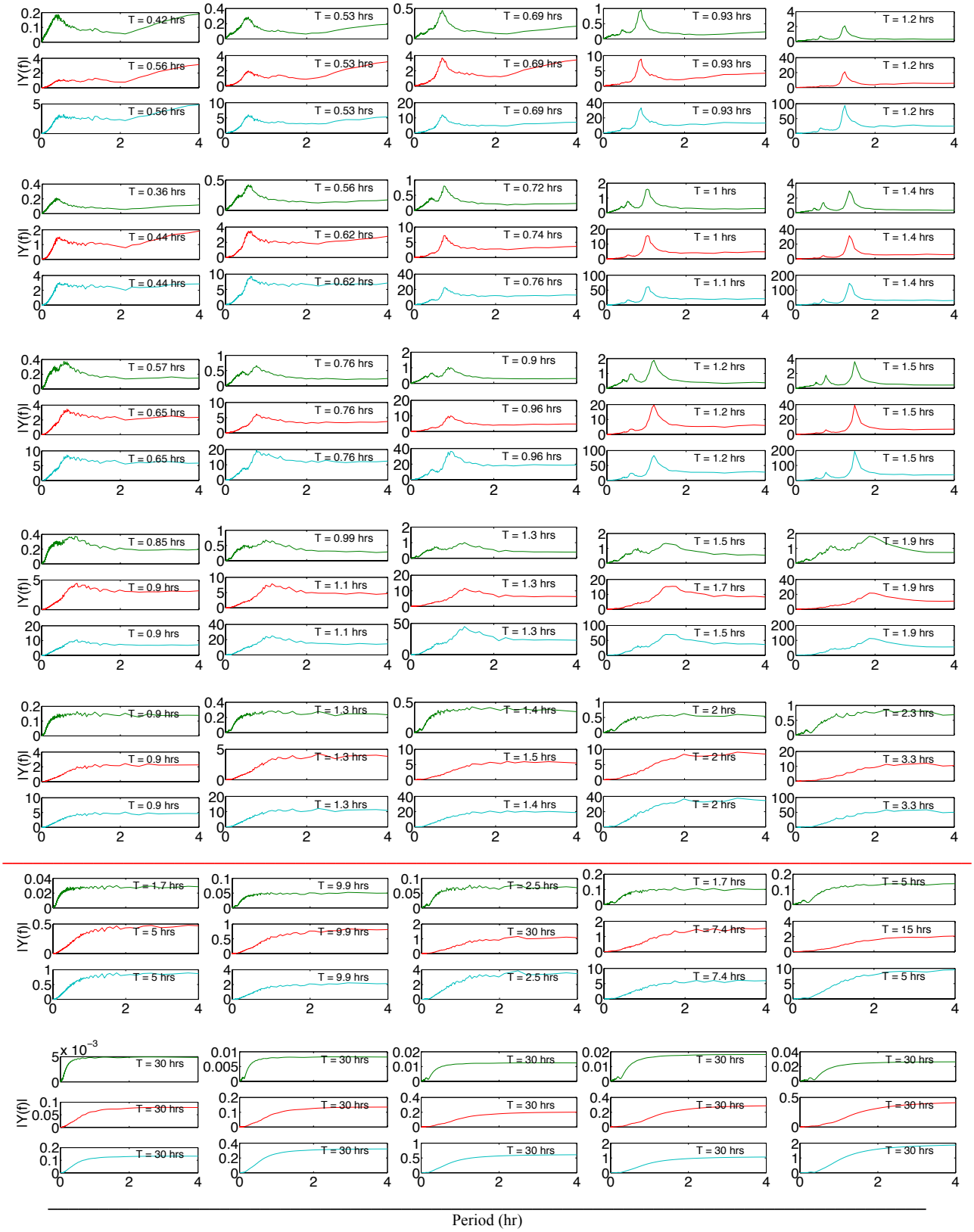

FIGURE S12 Period estimation from frequency spectra obtained by FFT averaged over 100 stochastic trajectories. Each row corresponds to a different feedback strength, from top to bottom: $\alpha = 10^8$ M^{-1}, $\alpha = 10^9$ M^{-1}, $\alpha = 10^{10}$ M^{-1}, $\alpha = 10^{11}$ M^{-1}, $\alpha = 10^{12}$ M^{-1}, $\alpha = 10^{13}$ M^{-1} and $\alpha = 10^{14}$ M^{-1}. Each column corresponds to a different transcription delay, from left to right: $\tau_1 = 100$ s, $\tau_1 = 300$ s, $\tau_1 = 500$ s, $\tau_1 = 800$ s and $\tau_1 = 1200$ s. Protein, mRNA and dimer are shown in red, green and teal, respectively. Period estimation becomes unreliable beyond $\alpha = 10^{12}$ M^{-1} (*red horizontal line*), marking the borderline with the burst expression regime.

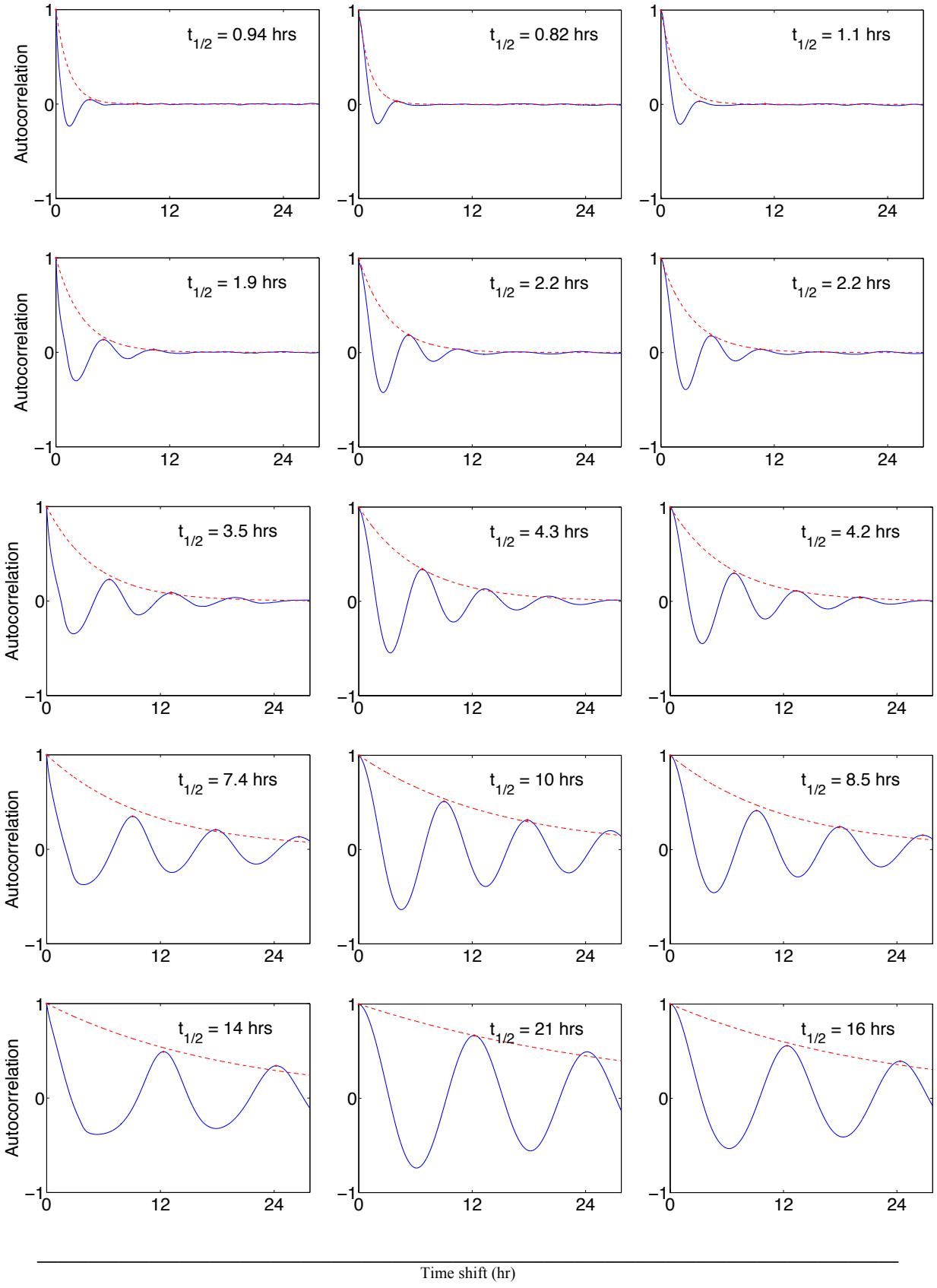

FIGURE S13 Autocorrelation function half-lives measure memory loss of stochastic oscillations. Each panel shows autocorrelation averaged over 100 stochastic trajectories and its half-lives $t_{1/2}$ for feedback strength fixed at $\alpha = 10^8$ M^{-1}. mRNA, protein and dimer are shown in left, center and right columns, respectively. Each row corresponds to a different feedback transcription delay, from top to bottom: $\tau_1 = 100$ s, $\tau_1 = 300$ s, $\tau_1 = 500$ s, $\tau_1 = 800$ s and $\tau_1 = 1200$ s.

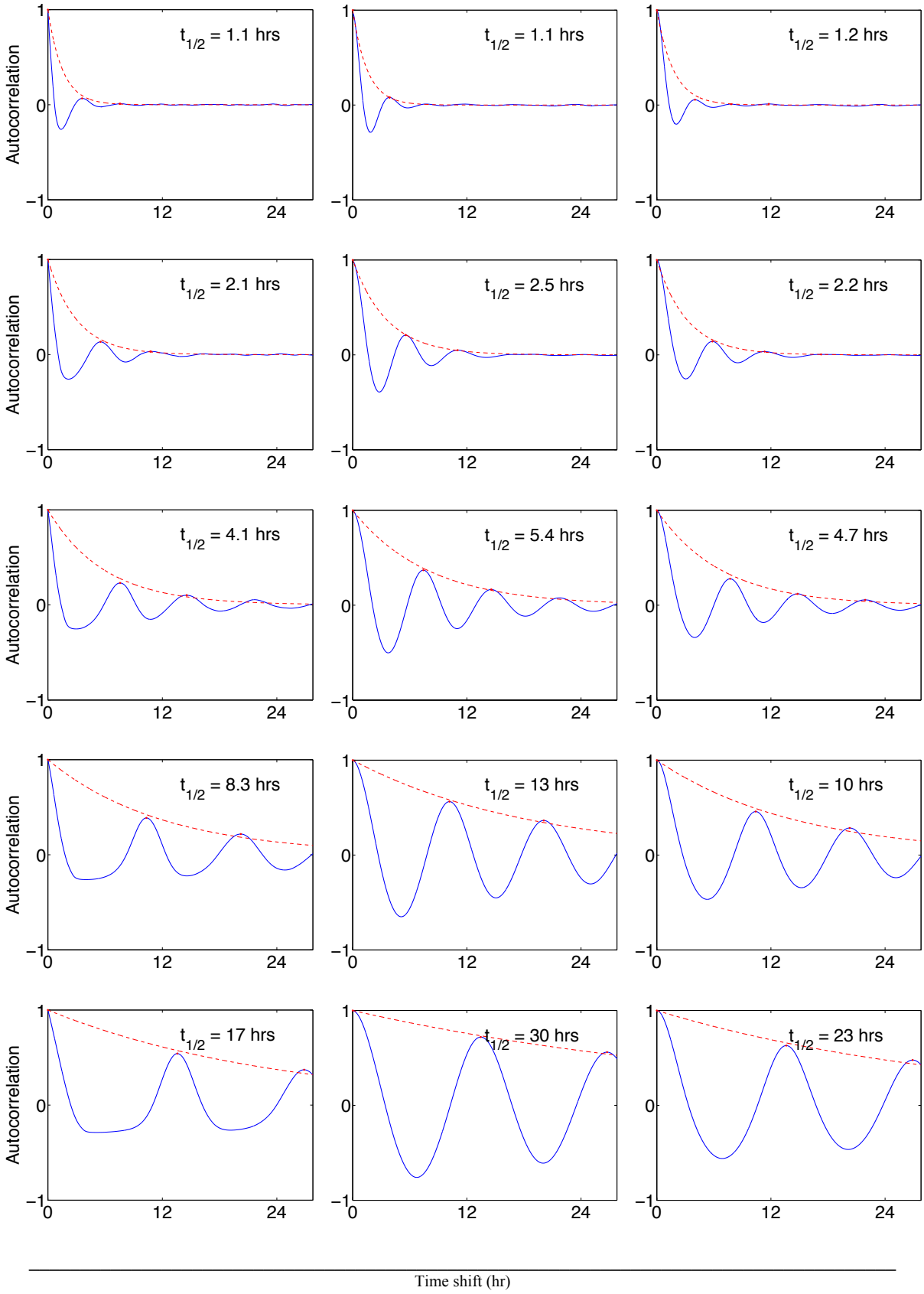

FIGURE S14 Autocorrelation function half-lives measure memory loss of stochastic oscillations. Each panel shows autocorrelation averaged over 100 stochastic trajectories and its half-lives $t_{1/2}$ for feedback strength fixed at $\alpha = 10^9$ M^{-1}. mRNA, protein and dimer are shown in left, center and right columns, respectively. Each row corresponds to a different feedback transcription delay, from top to bottom: $\tau_1 = 100$ s, $\tau_1 = 300$ s, $\tau_1 = 500$ s, $\tau_1 = 800$ s and $\tau_1 = 1200$ s.

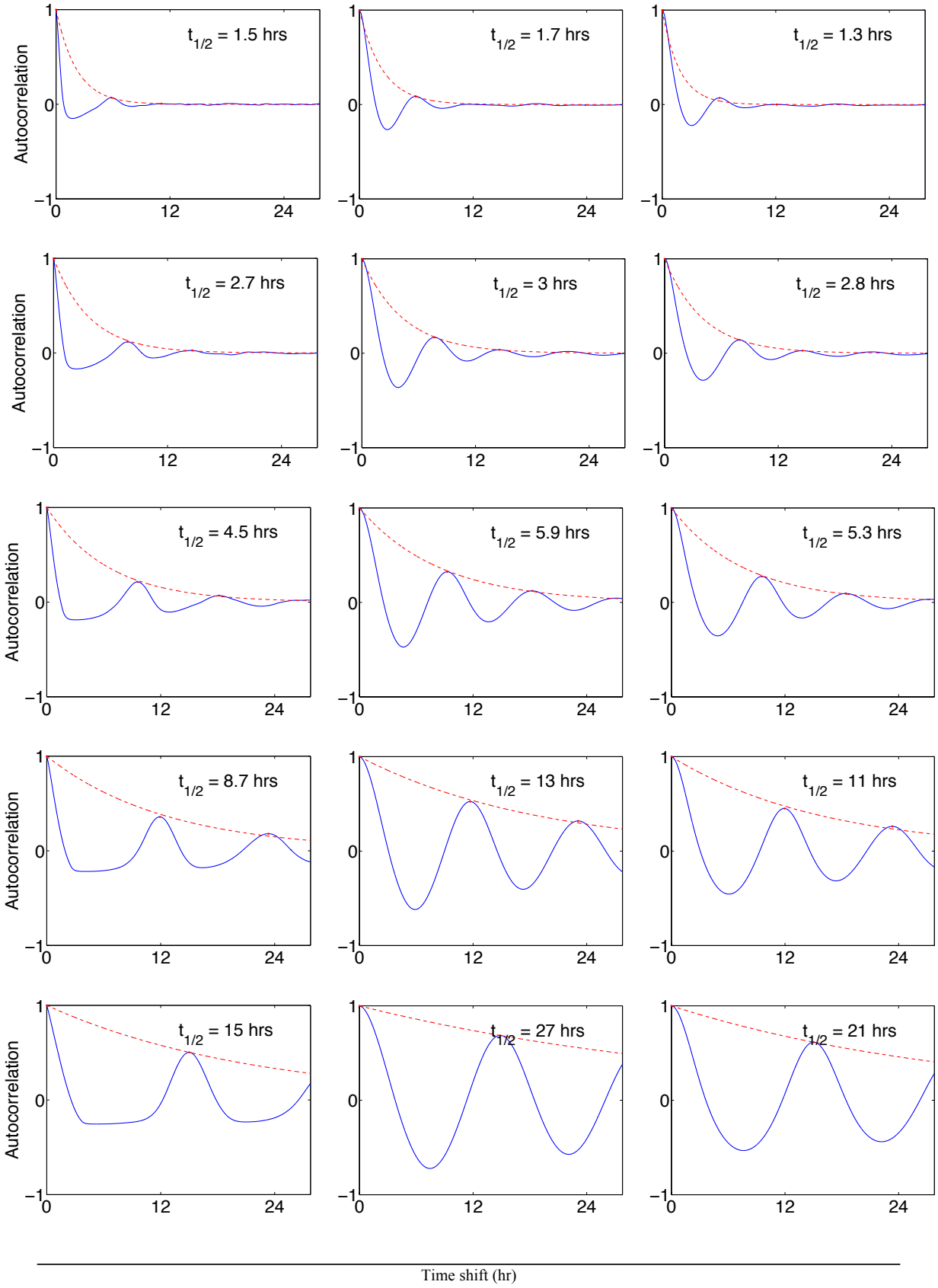

FIGURE S15 Autocorrelation function half-lives measure memory loss of stochastic oscillations. Each panel shows autocorrelation averaged over 100 stochastic trajectories and its half-lives $t_{1/2}$ for feedback strength fixed at $\alpha = 10^{10}$ M^{-1}. mRNA, protein and dimer are shown in left, center and right columns, respectively. Each row corresponds to a different feedback transcription delay, from top to bottom: $\tau_1 = 100$ s, $\tau_1 = 300$ s, $\tau_1 = 500$ s, $\tau_1 = 800$ s and $\tau_1 = 1200$ s.

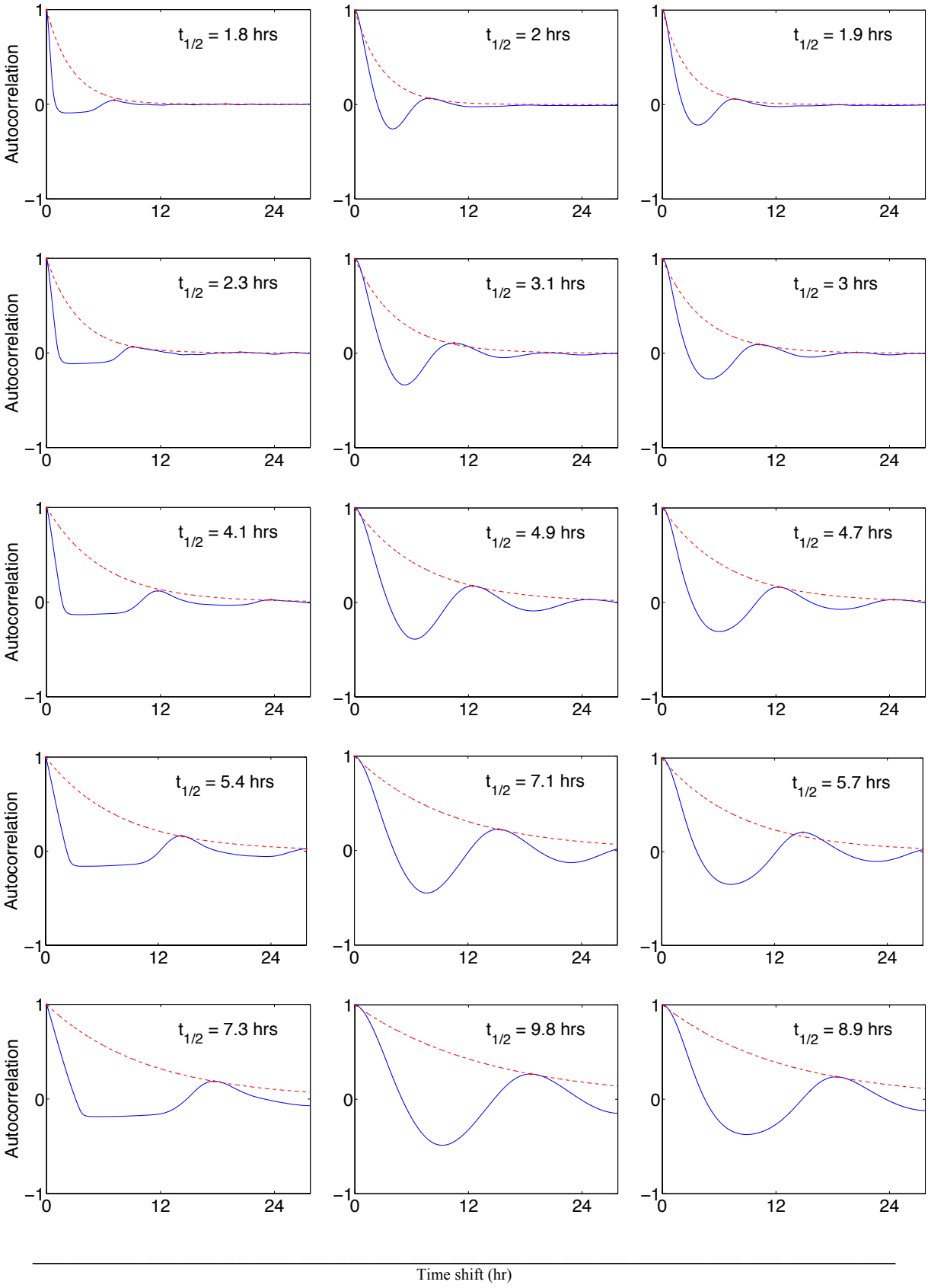

FIGURE S16 Autocorrelation function half-lives measure memory loss of stochastic oscillations. Each panel shows autocorrelation averaged over 100 stochastic trajectories and its half-lives $t_{1/2}$ for feedback strength fixed at $\alpha = 10^{11}$ M^{-1}. mRNA, protein and dimer are shown in left, center and right columns, respectively. Each row corresponds to a different feedback transcription delay, from top to bottom: $\tau_1 = 100$ s, $\tau_1 = 300$ s, $\tau_1 = 500$ s, $\tau_1 = 800$ s and $\tau_1 = 1200$ s.

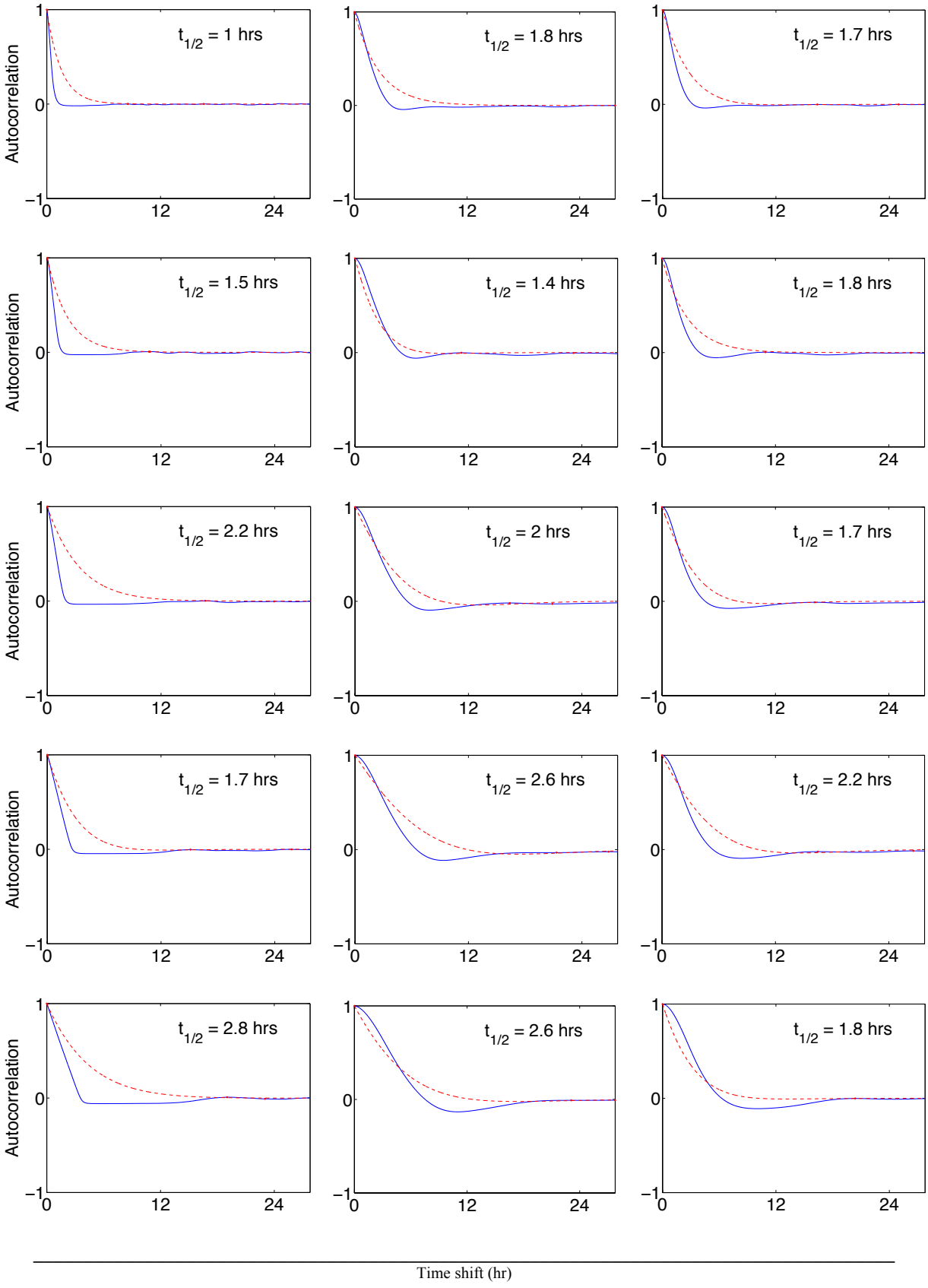

FIGURE S17 Autocorrelation function half-lives measure memory loss of stochastic oscillations. Each panel shows autocorrelation averaged over 100 stochastic trajectories and its half-lives $t_{1/2}$ for feedback strength fixed at $\alpha = 10^{12}$ M^{-1}. mRNA, protein and dimer are shown in left, center and right columns, respectively. Each row corresponds to a different feedback transcription delay, from top to bottom: $\tau_1 = 100$ s, $\tau_1 = 300$ s, $\tau_1 = 500$ s, $\tau_1 = 800$ s and $\tau_1 = 1200$ s.

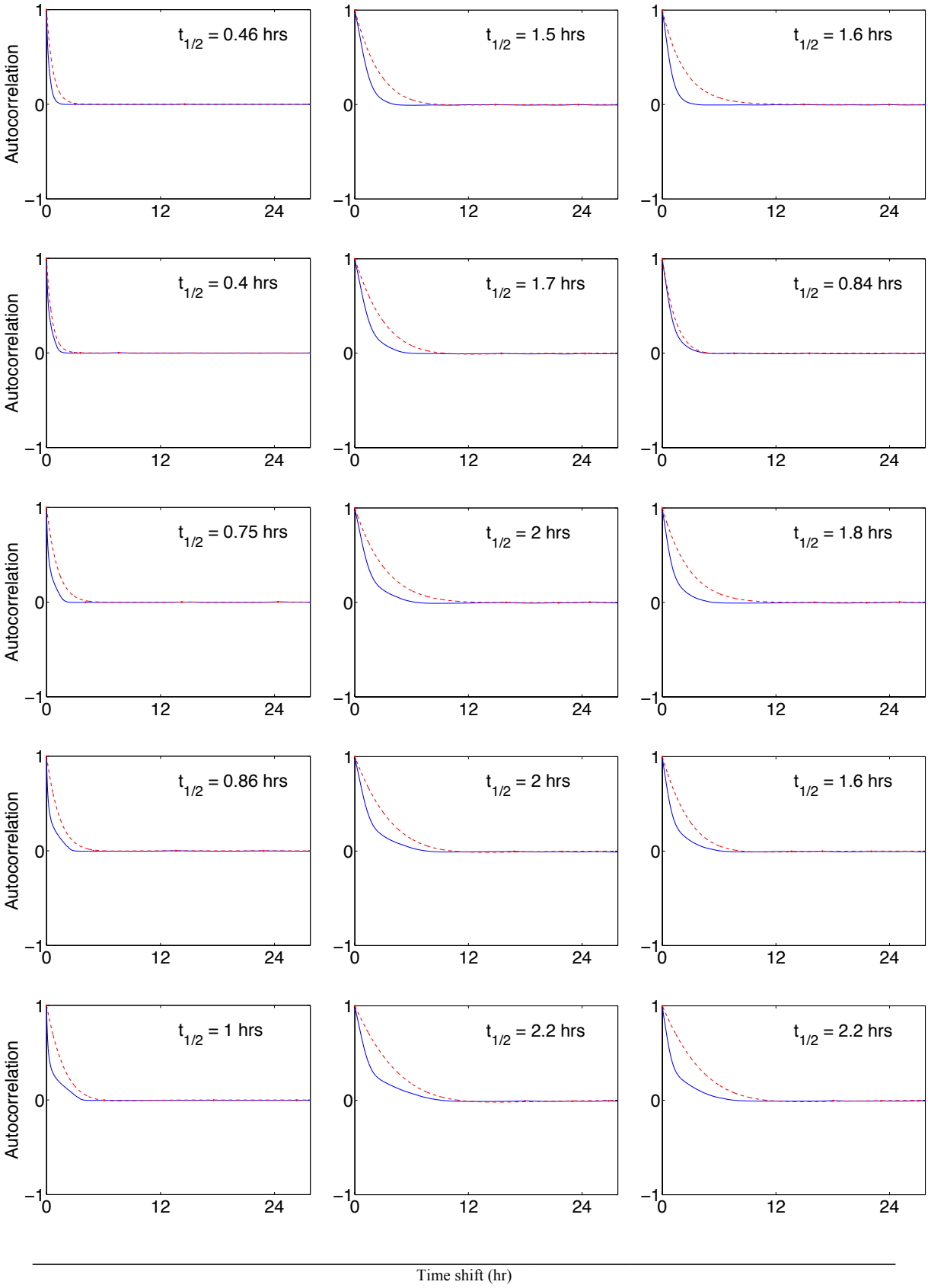

FIGURE S18 Autocorrelation function half-lives measure memory loss of stochastic oscillations. Each panel shows autocorrelation averaged over 100 stochastic trajectories and its half-lives $t_{1/2}$ for feedback strength fixed at $\alpha = 10^{13}$ M^{-1}. mRNA, protein and dimer are shown in left, center and right columns, respectively. Each row corresponds to a different feedback transcription delay, from top to bottom: $\tau_1 = 100$ s, $\tau_1 = 300$ s, $\tau_1 = 500$ s, $\tau_1 = 800$ s and $\tau_1 = 1200$ s.

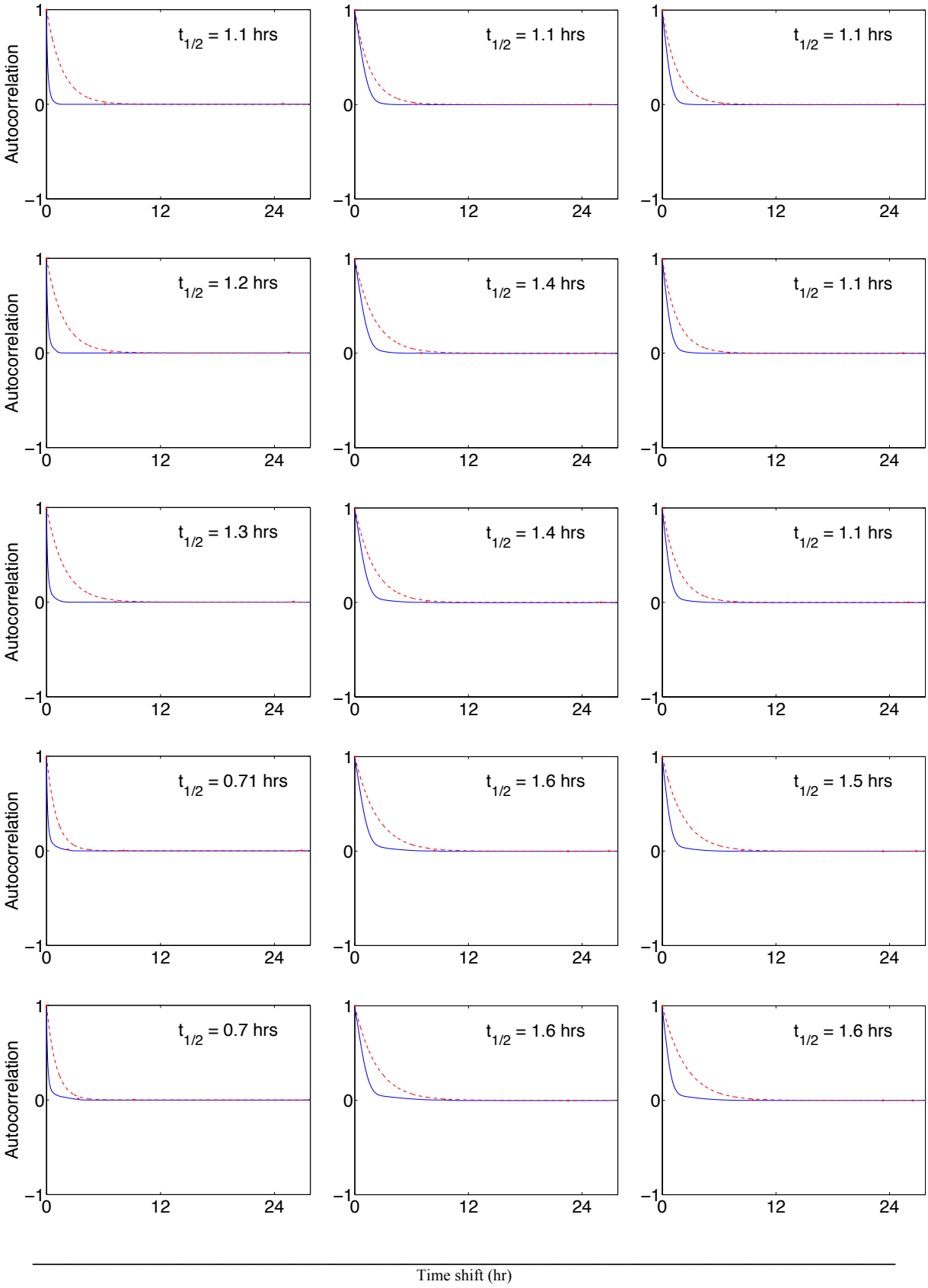

FIGURE S19 Autocorrelation function half-lives measure memory loss of stochastic oscillations. Each panel shows autocorrelation averaged over 100 stochastic trajectories and its half-lives $t_{1/2}$ for feedback strength fixed at $\alpha = 10^{14}$ M^{-1}. mRNA, protein and dimer are shown in left, center and right columns, respectively. Each row corresponds to a different feedback transcription delay, from top to bottom: $\tau_1 = 100$ s, $\tau_1 = 300$ s, $\tau_1 = 500$ s, $\tau_1 = 800$ s and $\tau_1 = 1200$ s.

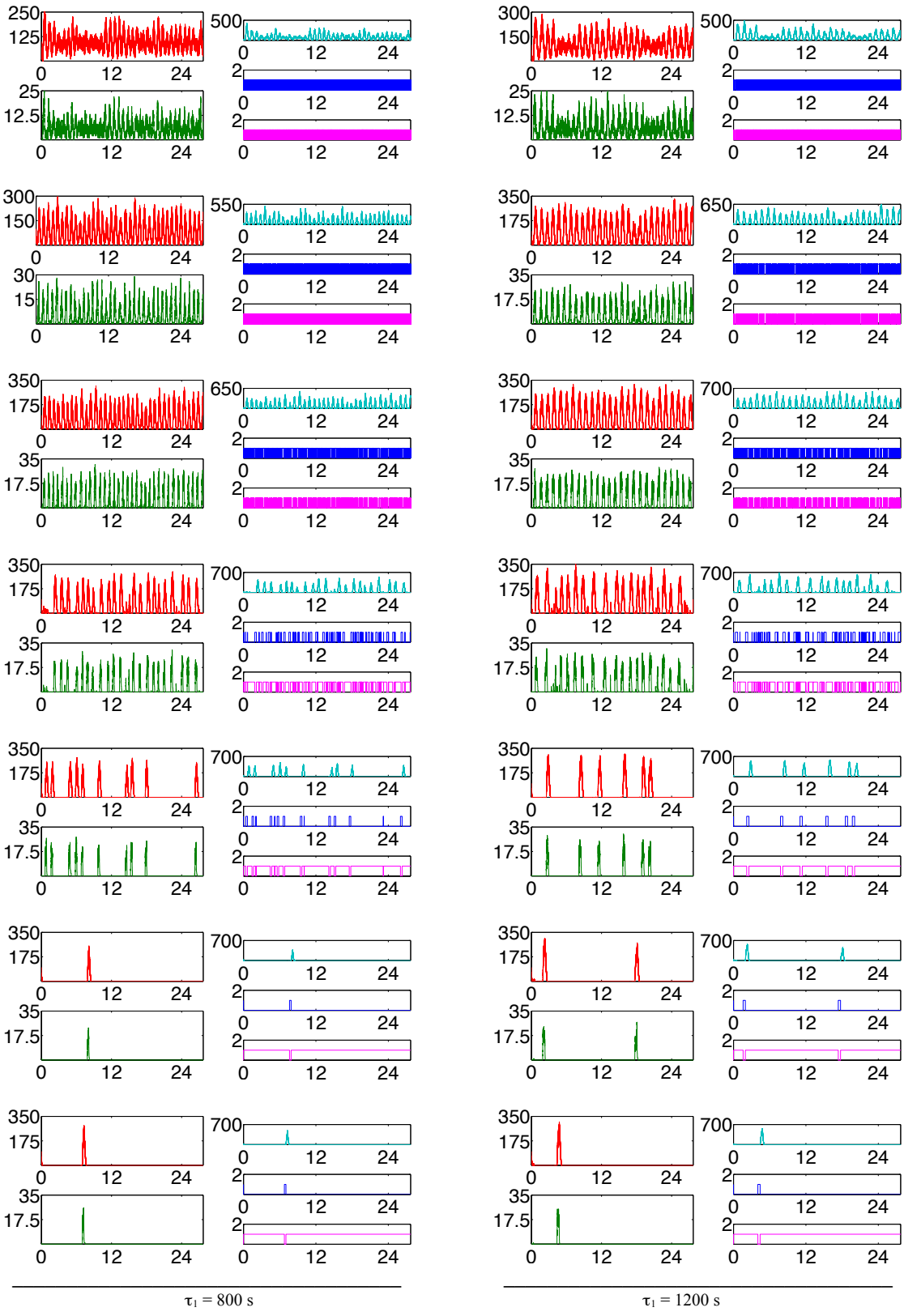

FIGURE S20 Sample stochastic trajectories showing oscillations (amount of molecules vs. hrs) for a 5 fL volume system. Each row corresponds to a different feedback strength, from top to bottom: $\alpha = 10^{8}$ M^{-1}, $\alpha = 10^{9}$ M^{-1}, $\alpha = 10^{10}$ M^{-1}, $\alpha = 10^{11}$ M^{-1}, $\alpha = 10^{12}$ M^{-1}, $\alpha = 10^{13}$ M^{-1} and $\alpha = 10^{14}$ M^{-1}. Each pair of columns was obtained with a different transcription delay: $\tau_1 = 800$ s, (*left*) and $\tau_1 = 1200$ s (*right*). The rest of parameter values were chosen as in Table S1. Protein, mRNA, dimer, DNA and the repressed complex are shown in red, green, teal, blue and pink, respectively.

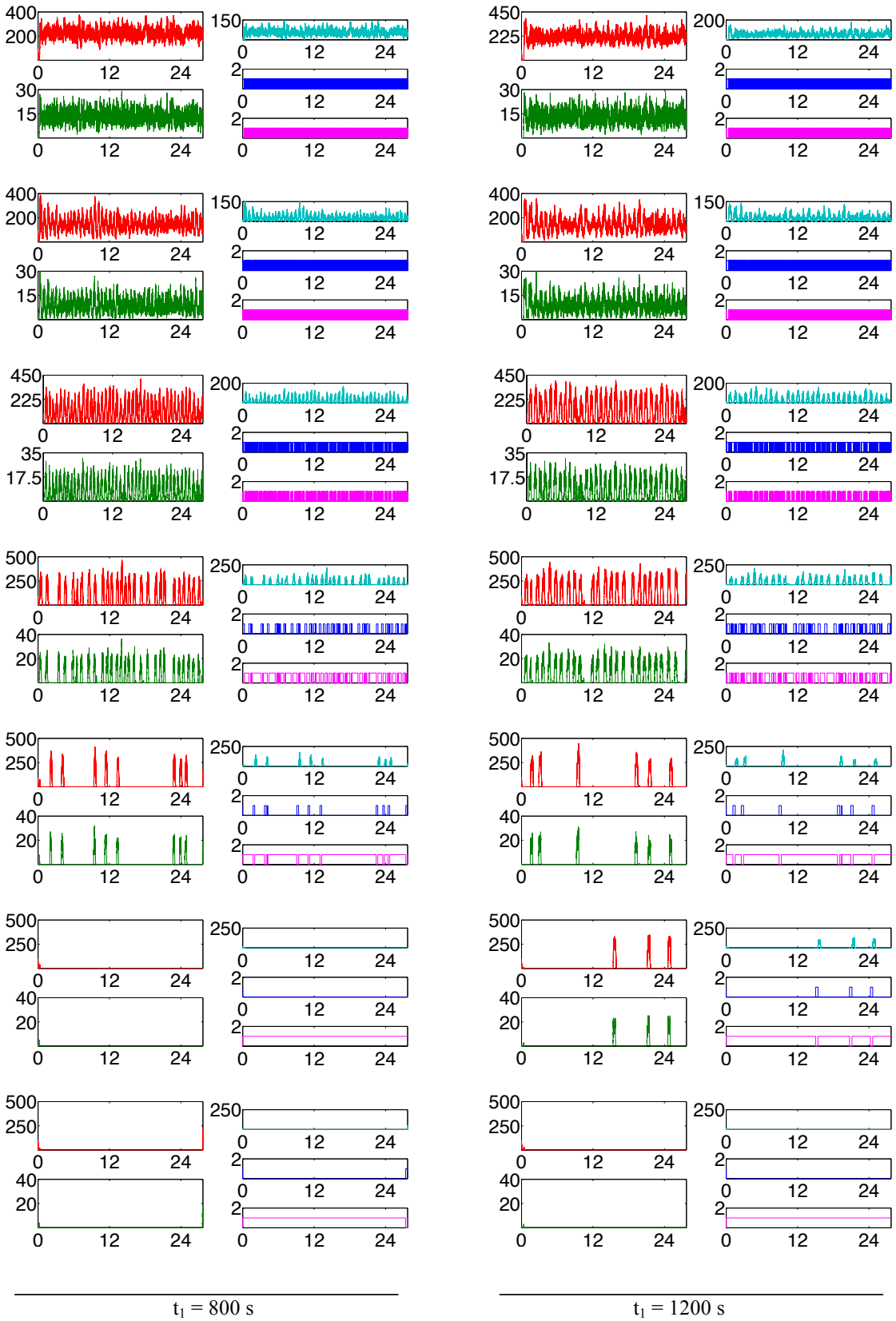

FIGURE S21 Sample stochastic trajectories showing oscillations (amount of molecules vs. hrs) for a 37 fL volume system. Each row corresponds to a different feedback strength, from top to bottom: $\alpha = 10^8$ M^{-1}, $\alpha = 10^9$ M^{-1}, $\alpha = 10^{10}$ M^{-1}, $\alpha = 10^{11}$ M^{-1}, $\alpha = 10^{12}$ M^{-1}, $\alpha = 10^{13}$ M^{-1} and $\alpha = 10^{14}$ M^{-1}. Each pair of columns was obtained with a different transcription delay: τ_1 = 800 s, (*left*) and τ_1 = 1200 s (*right*). The rest of parameter values were chosen as in Table S1. Protein, mRNA, dimer, DNA and the repressed complex are shown in red, green, teal, blue and pink, respectively.

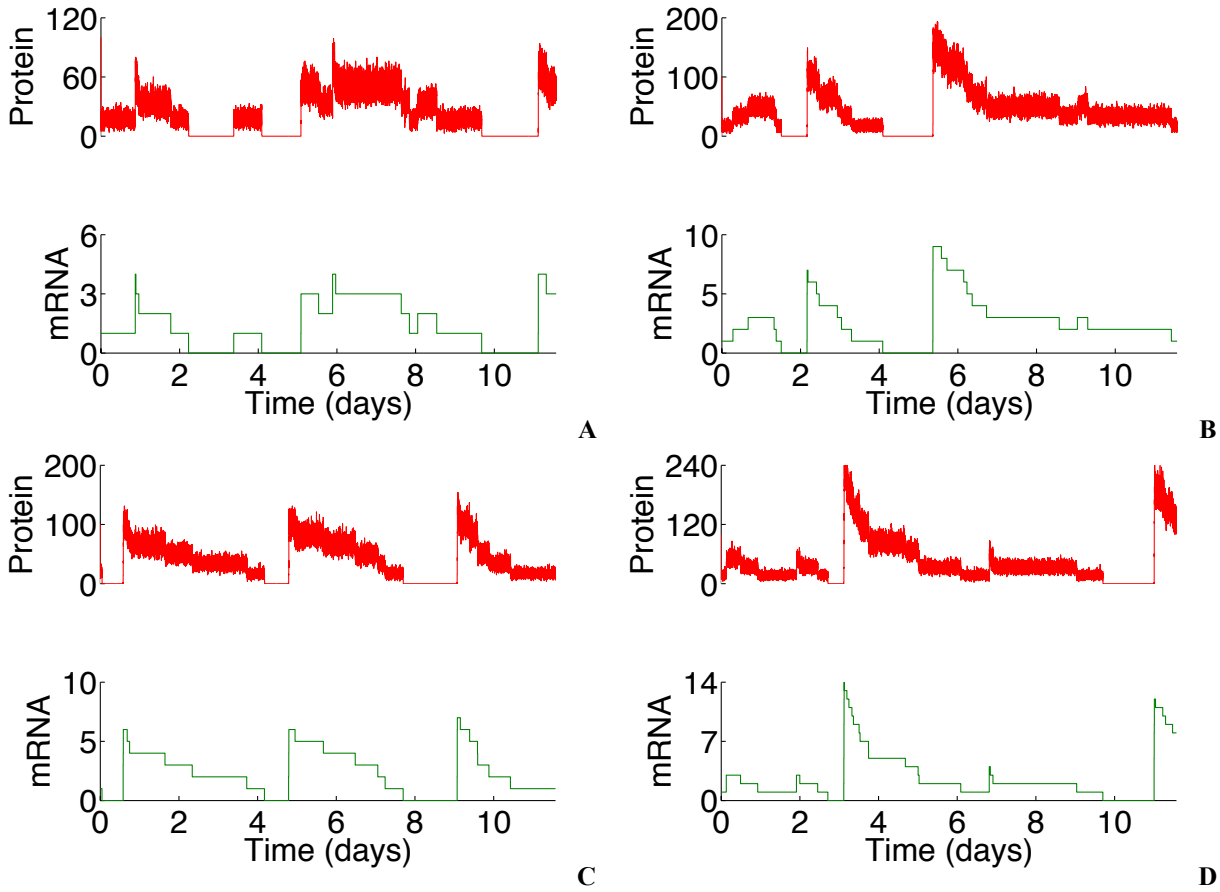

FIGURE S22 Protein and mRNA sample stochastic trajectories showing multimodality for a 5 fL volume system. Each panel corresponds to (A) $\tau_1 = 0$ s, $\tau_2 = 0$ s; (B) $\tau_1 = 100$ s, $\tau_2 = 100$ s; (C) $\tau_1 = 300$ s, $\tau_2 = 100$ s and (D) $\tau_1 = 500$ s, $\tau_2 = 100$ s. The rest of parameter values were chosen as in Table S2.

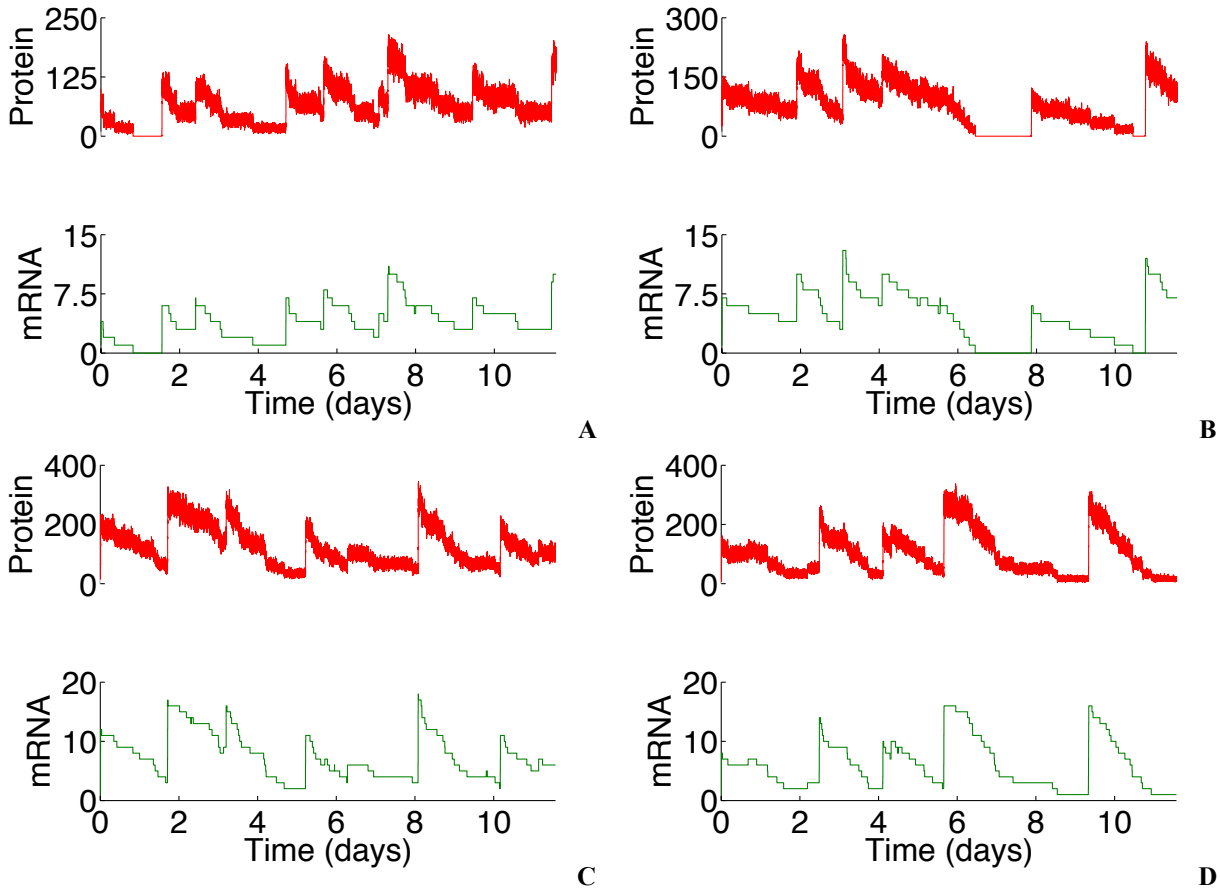

FIGURE S23 Protein and mRNA sample stochastic trajectories showing multimodality for a 37 fL volume system. Each panel corresponds to (A) $\tau_1 = 0$ s, $\tau_2 = 0$ s; (B) $\tau_1 = 100$ s, $\tau_2 = 100$ s; (C) $\tau_1 = 300$ s, $\tau_2 = 100$ s and (D) $\tau_1 = 500$ s, $\tau_2 = 100$ s. The rest of parameter values were chosen as in Table S2.

References for Supporting Material

1. Marquez-Lago, T. T., and J. Stelling. 2010. Counter-intuitive stochastic behavior of simple gene circuits with negative feedback. Biophysical journal 98:1742-1750.
2. Monk, N. A. M. 2003. Oscillatory Expression of Hes1, p53, and NF-κB Driven by Transcriptional Time Delays. Current Biology 13:1409-1413.
3. Kubitschek, H., and J. Friske. 1986. Determination of bacterial cell volume with the Coulter Counter. Journal of bacteriology 168:1466-1467.
4. Tyson, C. B., P. G. Lord, and A. E. Wheals. 1979. Dependency of size of Saccharomyces cerevisiae cells on growth rate. Journal of bacteriology 138:92-98.
5. Kuznetsov, I. U. A. 1998. Elements of applied bifurcation theory. Springer.
6. Cai, X. 2007. Exact stochastic simulation of coupled chemical reactions with delays. The Journal of chemical physics 126:124108.
7. Barrio, M., K. Burrage, A. Leier, and T. Tian. 2006. Oscillatory regulation of Hes1: discrete stochastic delay modelling and simulation. PLoS computational biology 2:e117.